ASM | Journal of Virology

| Host-Microbial Interactions | Full-Length Text

Residues E124, K129, and R134 in eEF1A domain I promote ALV-J replication via association with reverse transcriptase

Sheng Chen,[1,2,3] Liyi Chen,[1,2,3] Huijuan Xu,[1,2,3] Liguo Gao,[1,2,3] Yiming Yan,[4] Hongxing Li,[1,2,3] Xinheng Zhang,[1,2,3] Feng Chen,[1,2,3] Weiguo Chen,[1,2,3] Qingmei Xie[1,2,3]

AUTHOR AFFILIATIONS See affiliation list on p. 25.

ABSTRACT Subgroup J avian leukosis virus (ALV-J) is an oncogenic retrovirus posing significant threats to the global poultry industry. While host factors are known to regulate retroviral reverse transcription, the specific host proteins that support this critical step in ALV infection have remained completely unknown. In this study, we confirmed that overexpression or knockdown of eEF1A significantly enhanced or suppressed ALV-J proliferation, respectively. Co-immunoprecipitation and molecular docking demonstrated an association between eEF1A and the ALV-J reverse transcriptase (RT). Furthermore, three conserved residues in eEF1A domain I, including glutamate 124 (E124), lysine 129 (K129), and arginine 134 (R134), were identified as critical for the eEF1A-RT association. Alanine substitution at these EKR residues disrupted the eEF1A-RT association, markedly impairing viral reverse transcription and infectious virion production. From the viral perspective, a conserved tryptophan (W250) in the RT thumb domain acts as the key counterpart to the eEF1A EKR motif, and its mutation similarly abolishes the association and viral replication. Notably, this eEF1A-RT association and its functional significance are conserved across ALV subgroups A, B, K, and J. Together, our work elucidates that three residues E124, K129, and R134 within domain I of eEF1A mediate the association with ALV-J RT, promoting viral replication by enhancing reverse transcription efficiency. This finding provides the first mechanistic insight into host-dependent regulation of reverse transcription in ALV infection, broadens the understanding of how retroviruses co-opt host factors to facilitate this critical process, and provides a rational basis for genome editing of eEF1A to generate broad-spectrum ALV-resistant poultry lines.

IMPORTANCE Avian leukosis viruses (ALVs) cause severe economic losses to the global poultry industry, and current disease-resistant strategies targeting viral entry receptors only work for specific subgroups. This study identifies that the host protein eEF1A associates with ALV reverse transcriptase via conserved key residues to promote viral reverse transcription and replication, and this regulatory mechanism is conserved across multiple ALV subgroups. These findings provide a novel target for developing broad-spectrum ALV-resistant poultry breeds through genome editing, with important implications for poultry disease control.

KEYWORDS subgroup J avian leukosis virus, eukaryotic elongation factor 1A, reverse transcription, viral replication

Avian leukosis viruses (ALVs) are a family of avian oncogenic retroviruses that induce tumorigenesis and immunosuppression, leading to severe economic losses in global poultry production (1, 2). ALV in chickens are classified into seven subgroups, A–E, J, and K (2). Among these, subgroup J (ALV-J) is notably pathogenic and has been

Editor Viviana Simon, Icahn School of Medicine at Mount Sinai, New York, New York, USA

Address correspondence to Qingmei Xie, qmx@scau.edu.cn, or Weiguo Chen, wgchen81@scau.edu.cn.

The authors declare no conflict of interest.

See the funding table on p. 25.

Received 17 June 2026
Accepted 18 September 2026
Published 23 October 2026

Copyright © 2026 Chen et al. This is an open-access article distributed under the terms of the Creative Commons Attribution 4.0 International license.

responsible for severe outbreaks in commercial flocks over recent decades (3, 4). ALV-J is the typical member of the *Retroviridae* family with a genome comprising three principal coding genes: *gag*, *pol*, and *env* (2). The replication cycle of ALV-J follows the classic retroviral paradigm (5). In brief, it begins with receptor-mediated entry and uncoating, followed by reverse transcription of the viral RNA genome into double-stranded DNA. This proviral DNA is then integrated into the host genome and finally the production, assembly, and release of new virions (6, 7).

The hallmark and essential step of the retroviral life cycle is the reverse transcription of the viral RNA genome into double-stranded DNA, a process catalyzed by the reverse transcription complex (RTC) (8, 9). The RTC consists of viral components and various host proteins, with reverse transcriptase (RT) serving as its core enzymatic activity. Accumulating evidence demonstrates that host factors play an indispensable role in regulating retroviral reverse transcription. Evidence from an avian sarcoma/leukosis virus-based cell-free system demonstrated that complete viral DNA synthesis occurs only upon the addition of cell lysates, highlighting the essential contribution of host factors (10). Subsequent studies have demonstrated that the reverse transcription of retroviruses such as human immunodeficiency virus (HIV) and murine leukemia virus (MLV) is modulated by specific host factors interacting with their RT. These findings highlight the diversity in regulatory mechanisms across different retroviruses and the distinct host proteins involved. For example, the RNA-binding protein HuR associates with HIV RT and modulates early reverse transcription (11), whereas eRF1 binds the RT of MLV, but not that of HIV (12). Other host factors, including the antiviral protein APOBEC3G (13), uracil DNA glycosylase UNG2 (14), and the kinase-anchoring protein AKAP149 (15), have also been implicated in regulating reverse transcription efficiency. While several cellular factors that modulate reverse transcription in HIV and MLV have been identified (11–15), the key host proteins supporting this essential step in ALV remain largely unknown.

The identification of host proteins encapsulated within mature virions represents a robust strategy for elucidating the regulatory mechanisms of the viral life cycle (16–18). For example, proteomic profiling of purified hepatitis C virus particles reveals an essential role for the nucleoporin Nup98 in virus morphogenesis (18). In our previous study, we employed subtilisin digestion combined with nanoscale liquid chromatography-tandem mass spectrometry to conduct proteomic sequencing of host proteins packaged in purified ALV-J virions (19). Across two independent replicates, the host protein eukaryotic elongation factor 1A (eEF1A) was consistently detected with remarkable abundance and high confidence, prompting further investigation into its role during viral replication. eEF1A primarily functions in protein synthesis by delivering aminoacyl-tRNAs to the ribosome during the translation elongation phase (20). Beyond translation, it participates in various noncanonical cellular processes, including protein degradation and apoptosis (21, 22). Notably, eEF1A has been shown to regulate the infection cycles of numerous viruses, often by interacting with viral proteins or viral genomes to influence viral replication and pathogenicity. For example, eEF1A silencing suppresses nucleocapsid protein expression in coronavirus, inhibiting viral proliferation (23). In flaviviruses, eEF1A associates with the replication complex and promotes negative-strand RNA synthesis by facilitating interactions between the viral genome and replication machinery (24). Interestingly, eEF1A regulates multiple stages of the HIV-1 life cycle by interacting with distinct viral components (25–28). For example, eEF1A interacts with the 5′ untranslated region of HIV-1 genomic RNA, and the interaction is important for late DNA synthesis in reverse transcription (28). Additionally, eEF1A has been reported to directly interact with the HIV-1 RT to modulate reverse transcription efficiency (29). Despite these broad connections, the functional significance of eEF1A in ALV-J infection, and particularly its role in specific steps of the viral life cycle, remains unclear.

In this study, we demonstrate that eEF1A associates with ALV-J RT via three key residues (E124, K129, and R134) in its domain I. From the viral side, we identify tryptophan 250 (W250) in the RT thumb domain as the counterpart important for this

association. Disruption of this interface severely impairs reverse transcription and viral replication, and this regulatory mechanism is conserved across ALV subgroups A, B, K, and J. This work deepens our understanding of ALV reverse transcription and identifies residues E124, K129, and R134 in eEF1A as potential targets for broad-spectrum anti-ALV strategies.

MATERIALS AND METHODS

Virus, cells, and antibodies

DF-1 cell lines, preserved in our laboratory, were grown in Dulbecco's modified Eagle medium (DMEM) supplemented with 10% fetal bovine serum and 1% penicillin-streptomycin and maintained at 37°C and 5% CO_2. The ALV-A GD08 strain was a generous gift from Professor Weisheng Liao of South China Agricultural University. The ALV-B SDAU09C2 strain and ALV-K JS11C1 were kindly donated by Professor Peng Zhao of Shandong Agricultural University. The ALV-J SCAU1903 strain was conserved in our laboratory.

Virus titers were determined by 50% tissue culture infectious dose ($TCID_{50}$) assay. Briefly, DF-1 cells were seeded in 96-well plates at a density of 1×10^4 cells per well 24 h prior to infection. Ten-fold serial dilutions of virus stock were prepared in DMEM, and 100 µL of each dilution was added to eight replicate wells. Plates were incubated at 37°C with 5% CO_2 for 72 h. Infection-positive wells were identified by indirect immunofluorescence using an anti-gp37 antibody, and wells exhibiting specific green fluorescence were scored as positive. $TCID_{50}$ values ($TCID_{50}$/mL) were calculated using the Reed-Muench method. The multiplicity of infection (MOI) was defined based on $TCID_{50}$ infectious units, calculated as the ratio of total virus infectious units to the number of seeded cells: MOI = (viral titer in $TCID_{50}$/mL × inoculation vol) / total cell number per well. For all paired comparisons between rALV-J and rALV-J-W250A, viral inocula were normalized to equivalent $TCID_{50}$ units to ensure equal infectious input.

The antibodies used for Western blot, immunoprecipitation, and confocal microscopy analyses were as follows: anti-GFP polyclonal antibody (Ab) (Abcam, ab183734), anti-mCherry polyclonal Ab (ABclonal, AE002), anti-eEF1A monoclonal Ab (Abcam, EPR9471), anti-Flag monoclonal Ab (ABclonal, AE092), anti-HA monoclonal Ab (ABclonal, AE008), anti-β-actin monoclonal Ab (Epizyme, LF201), and anti-gp37 polyclonal Ab and anti-p68 polyclonal Ab (Sangon Biotech). A protein molecular weight marker (Epizyme, WJ102) was used.

Plasmids and mutagenesis

Chicken eEF1A was cloned from the cDNA of DF-1 cells using specific primers and was cloned into the pRK5 plasmid with an HA tag. The plasmids expressing different eEF1A domains, including eEF1A-DI, eEF1A-DII, eEF1A-DIII, eEF1A-DI + II, eEF1A-DII + III, eEF1A-1-56 AA del, eEF1A-120-135 AA del, and eEF1A-1-135 AA del, were also cloned into the pRK5 plasmid with an HA tag by homologous recombination reactions. The eukaryotic expression plasmids based on the ALV-J SCAU1903 RT template, including pRK5-RT, -RT-ΔR, -RT-ΔR+C, -RT-ΔR+C+T, -RT-R, -RT-R+C, and -RT-R+C+T, were all constructed with an mCherry tag. All constructs were verified by Sanger sequencing. The primers for constructing all plasmids and mutants are referenced in Table S1.

Generation of ALV-J mutant

The DNA fragment of the whole proviral genome of SCAU1903 and the linearized pVAX1 vector were processed by homologous recombination to rescue the recombinant virus. In brief, three fragments of proviral cDNA of the SCAU1903 strain and the linearized pVAX1 vector were generated by PCR and then fused using the Clon Express Ultra One Step Cloning Kit (Vazyme). DF-1 cells were transfected with proviral DNA, and the virus was rescued. The RT W250 site was mutated in the pVAX-ALV-SCAU1903-wt to rescue the

mutated recombinant virus. The rescued viruses were named rALV-J and rALV-J-W250A. The titer of the rescued recombinant virus was determined based on the $TCID_{50}$ value using the Reed and Muench method.

Virion purification

DF-1 cells were infected with rALV-J or rALV-J-W250A at an MOI of 0.01, and cell culture supernatants were harvested at 72 hours post-infection (hpi). Supernatants were first clarified by centrifugation at 4,000 × *g* for 10 min at 4°C to remove cell debris, followed by filtration through a 0.45-µm pore-size filter. Viral particles were concentrated by ultracentrifugation at 100,000 × *g* for 2 h at 4°C (Beckman SW41 rotor). The crude viral pellets were gently resuspended in ice-cold PBS overnight at 4°C and then further purified by ultracentrifugation through a 20% (wt/vol) sucrose cushion at 110,000 × *g* for 1.5 h at 4°C to remove soluble contaminating proteins. The final virion pellets were resuspended in ice-cold PBS. The total protein concentration of purified virions was determined by bicinchoninic acid assay, and equal amounts of total viral protein were loaded for SDS-PAGE. Coomassie brilliant blue staining was performed in parallel to verify equal loading.

RNA interference and shRNA knockdown

siRNA targeting eEF1A and control siRNA were applied to DF-1 cells using Lipofectamine RNAiMAX according to the manufacturer's instructions (Invitrogen). siRNA sequences for knockdown of eEF1A included siRNA#1 (sense, 5′-CUACAAAAUUGGUGGCAUUTT-3′), siRNAi#2 (sense, 5′-GCACUUACAUCAAGAAAAUTT-3′), siRNA#3 (sense, 5′-CCAAAUCA-GUGCUGGUUAUTT-3′), and negative siRNA control (sense, 5′-UUCUCCGAACGUGUCAC-GUTT-3′).

CRISPR-Cas9-mediated knockout

The eEF1A sgRNA was designed using the Synthego CRISPR Design Tool to target exon 2 of the chicken eEF1A gene (GenBank accession number: NM_001321516.2). The sgRNA target sequence is 5′-AATGTGGTGGCATCGACAAG-3′ (PAM: AGG). Complementary oligo duplexes were cloned into the lentiviral vector GV392 carrying the Cas9 expression cassette. Lentivirus was packaged in 293T cells, and titers were determined by quantitative PCR. DF-1 cells were transduced with lentivirus for 12 h and then cultured in DMEM with 2% FBS for 72 h, followed by selection with 2 µg/mL puromycin. Genomic DNA was extracted from puromycin-selected cells, and the target locus was amplified using the following primers: forward 5′-ATGGGAAAGGAGAAGACCCA-3′, reverse 5′-TCGA TGATGGTGACGTAGTAC-3′. Amplicon libraries were subjected to HI-TOM sequencing with an average effective sequencing depth of approximately 2,000×. Editing efficiency was quantified as the proportion of reads containing insertions or deletions (indels) at the target site relative to total amplifiable reads.

Virus production and quantification

Supernatants were collected at 24, 48, 72, and 120 hpi. Viral capsid protein (CA) levels were measured using a commercial ALV p27 CA ELISA kit (IDEXX Laboratories) following the manufacturer's instructions. All enzyme-linked immunosorbent assays (ELISAs) were performed in triplicate with standard curves.

Western blot and co-immunoprecipitation (Co-IP)

DF-1 cells expressing various wild-type or mutant proteins were lysed in RIPA buffer supplemented with protease inhibitor cocktail. The lysate was cleared by centrifugation at 12,000 × *g* for 20 min at 4°C. For co-immunoprecipitation, supernatants were incubated with anti-Flag magnetic beads (for viral protein bait) or anti-HA magnetic beads (for eEF1A bait) for 12 h at 4°C. Beads were washed three times with TBST

buffer, and bound proteins were eluted with SDS loading buffer. Western blotting was performed using the indicated primary antibodies, followed by horseradish peroxidase-conjugated goat anti-mouse or goat anti-rabbit secondary antibodies. Protein bands were visualized using a C600 ultrasensitive chemiluminescence imager under nonsaturating linear exposure conditions. Protein molecular weight markers (epizyme, WJ102) were run in parallel on all gels, and the expected band sizes are annotated in each figure. Uncropped full-length blot images are provided in the supplementary materials. All Western blot assays for total eEF1A protein were performed with anti-eEF1A monoclonal antibody (Abcam, EPR9471) under linear exposure conditions to ensure quantitative consistency between band intensity and protein abundance. Exogenously expressed HA-tagged eEF1A was detected using anti-HA monoclonal antibody (ABclonal, AE008). Of note, the HA tag adds only ~1 kDa to the molecular weight of eEF1A, so total eEF1A antibody staining presents as a single band in overexpression samples, reflecting the sum of endogenous and exogenous eEF1A protein.

Indirect immunofluorescent assay (IFA)

DF-1 cells were infected with ALV-J SCAU1905 at 37°C with 5% CO_2 for 2 h. After incubation, cells were washed three times with PBS at room temperature and fixed with 1% paraformaldehyde for 15 min at room temperature. Then, cells were washed three times with PBS at room temperature and fixed with 0.1% triton X-100 for 15 min at room temperature. After washing three times, the cells were incubated with mouse anti-gp37 antibody at a dilution of 1:100 in PBS for 1 h at 37°C. This was followed by washing and then incubation with 1:100 dilution of a fluorescein isothiocyanate-conjugated secondary antibody (FITC-conjugated goat anti-mouse IgG antibody) for 1 h at 37°C. After three washes with PBST, DF-1 cells were visualized using a fluorescence microscope. Normal DF-1 cells were used as negative controls.

Confocal microscopy

DF-1 cells were transfected with pRK5-mCherry-eEF1A and EGFP-RT or EGFP empty vector for 48 h. Then, cells were washed with PBS three times and fixed with 4% formaldehyde for 15 min at room temperature, followed by permeabilization with 0.1% Triton X-100 in PBS for 15 min. Samples were blocked with 5% skim milk at 37°C for 30 min before being incubated with mouse anti-HA (1:200) for 1 h at 37°C. Then, cells were washed three times with TBST and incubated with Alexa 594 anti-mouse secondary antibody (1:200). Finally, cells were stained with DAPI for 15 min at room temperature. Stained cells were subsequently analyzed using a Leica SP8 STED3X confocal laser scanning microscope.

Reverse transcription assay and qPCR

DF-1 cells were incubated with ALV-J SCAU1903 at 37°C for 2 h and then washed three times with PBS, and incubation was continued at 37°C for 6 h. The cells were washed three times with PBS and lysed using cell lysis buffer (100 mM Tris-HCL, 500 mM EDTA, and 10% SDS). The lysate was extracted once with an equal volume of phenol: chloroform: isoamyl alcohol (25:24:1) and once with chloroform. The extracts were ethanol-precipitated, washed with 70% (vol/vol) ethanol, and resuspended in 0.1 mM EDTA. The early and late reverse transcription products were analyzed by quantitative PCR. Early reverse transcription products (5′ R-U5 strong-stop cDNA) and late products (*pol* gene region) were quantified by qPCR. Primer positions relative to the ALV-J SCAU1903 genome are as follows: early primers (nt 12–180) and late primers (nt 2,482–2,615). Viral DNA copy numbers were normalized to the chicken *GAPDH* genomic locus. To eliminate input viral RNA contamination, nucleic acid samples were treated with RNase A prior to qPCR. No-template and uninfected cell controls were included in each run. For RTC fraction samples, equal volumes of each fraction were used as input. Primer sequences are as follows: early DNA copies (F: 5′-GCCATTTTACCTCCCACCAC-3′, R: 5′-AATGAAGCCTTCCGCT

TCAT-3′) and late DNA copies (F: 5′-AGCGGAAGGCTTCATTTGGT-3′, R: 5′-TATGACGGCTTCC ATGCTTG-3′).

Reverse transcriptase assay

The harvested samples were also assayed for RT activity using a colorimetric reverse transcriptase assay (11468120910, Roche Applied Science, Indianapolis, USA) according to the manufacturer's protocol.

Sucrose gradient RTC isolation

Purification of ALV-J RTCs was performed with minor modifications according to a previously described protocol for HIV RTC extraction (29). Briefly, infected DF-1 cells were harvested and washed twice with pre-chilled hypotonic lysis buffer. Cells were mechanically homogenized on ice to achieve gentle cell rupture. The lysate was then centrifuged at 12,000 rpm for 10 min at 4°C to pellet cell debris and nuclei, and the resulting post-nuclear supernatant was carefully recovered. The supernatant was layered onto the top of a pre-prepared linear 30%–60% (wt/wt) sucrose density gradient. Ultracentrifugation was carried out at 100,000 rpm for 8 h at 4 °C. Following centrifugation, the bottom of the centrifuge tube was pierced using a heated 21-gauge needle, and the gradient material was sequentially collected from bottom to top into 12 equal-volume fractions. Individual fractions were subsequently subjected to Western blot and qPCR analysis for protein and viral DNA detection, respectively.

Autodock analysis

The molecular models of the host protein eEF1A and ALV-J RT protein were calculated through homology modeling by the SWISS-MODEL server (https://swissmodel.expasy.org/). The molecular docking between ALV-J RT and eEF1A protein was conducted using the ClusPro server (https://cluspro.bu.edu/), employing the predicted models of eEF1A and ALV-J RT for the docking simulation. During the docking process, eEF1A was designated as the receptor and ALV-J RT as the ligand. The ligand was rotated 70,000 times, and with each rotation, it was translated relative to the receptor along the x, y, and z axes, selecting the best-scored result from each rotation. Out of the 70,000 rotations, this study selected the 1,000 rotation/translation combinations with the lowest scores. Subsequently, these 1,000 ligand positions were clustered using a 9 Å C-alpha RMSD radius to identify the most "adjacent" ligand positions within 9 Å, that is, the cluster centers. Finally, the top 10 cluster centers with the most cluster members were visually inspected one by one, and the most probable molecular contacts were further assessed. The PyMOL software was used to edit and generate the molecular graphics of the docking models.

Statistical analysis

Statistical analyses were performed using Student's *t*-test or one-way analysis of variance (ANOVA) from at least three independent experiments or measurements. Statistical significance was set at *, $P < 0.05$; **, $P < 0.01$; ***, $P < 0.001$.

RESULTS

eEF1A positively regulates ALV-J replication

In order to clarify the crucial role of host protein eEF1A in the ALV-J life cycle, we conducted eEF1A-knockdown (eEF1A-KD) of DF-1 cells using siRNA. Efficient reduction was confirmed at both mRNA and protein levels (Fig. S1A and B), with no effect on cell viability (Fig. S1C). In eEF1A-KD DF-1 cells, Western blot analysis revealed decreased levels of the viral transmembrane protein gp37 at 48 and 72 hpi (Fig. 1A and Fig. S1C). Measurement of viral particles in the culture supernatant showed that secretion of the ALV-J capsid protein (CA) was comparable between eEF1A-depleted and control cells

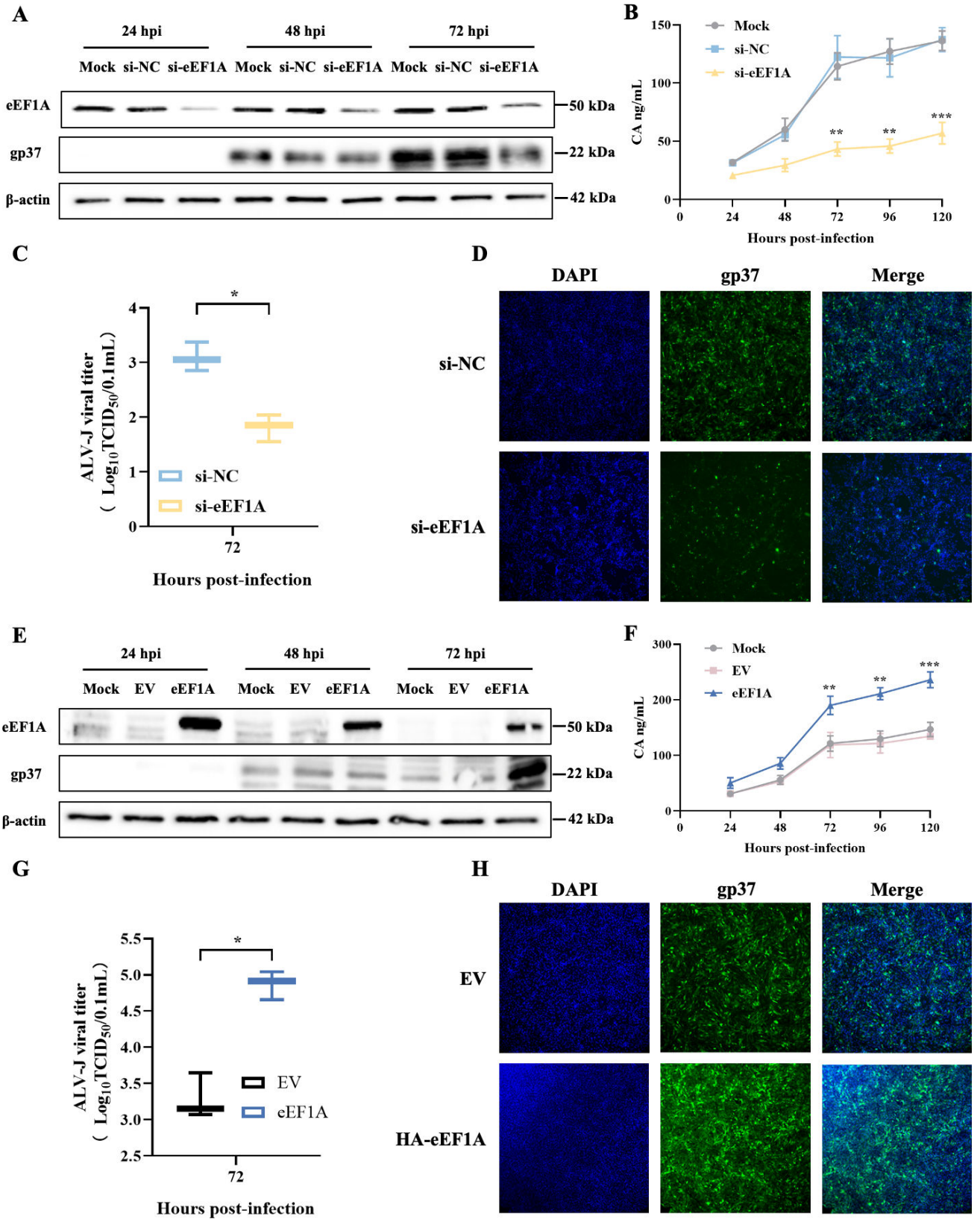

FIG 1 eEF1A positively regulates ALV-J replication. DF-1 cells were transfected with siRNA targeting eEF1A or eEF1A overexpression plasmids, along with si-NC or EV as negative controls, respectively. At 24 h post-transfection, cells were infected with ALV-J at an MOI of 0.01. (A) Western blot analysis of viral protein expression upon eEF1A depletion. Cell lysates were collected at 24, 48, and 72 hpi, and viral gp37 protein levels were detected by Western blotting using an

(Continued on next page)

Fig 1 (Continued)

anti-gp37 antibody. eEF1A protein levels were detected using anti-pan-eEF1A antibody. (B) ELISA analysis of viral CA secretion upon eEF1A depletion. Culture supernatants were collected at 0, 24, 48, 72, 96, and 120 hpi, and CA levels were measured using an ELISA kit. (C) Virus titer determination upon eEF1A depletion. Virus titers in culture supernatants were determined at 72 hpi using the Reed-Muench method. (D) Immunofluorescence analysis of gp37 expression upon eEF1A depletion. At 72 hpi, cells were fixed and stained with an anti-gp37 antibody. Representative images are shown (20× magnification). (E) Western blot analysis of viral protein expression upon eEF1A overexpression. Cell lysates were collected at 24, 48, and 72 hpi, and viral gp37 protein levels were detected by Western blotting using an anti-gp37 antibody. eEF1A protein levels were detected using anti-HA antibody. (F) ELISA analysis of viral CA secretion upon eEF1A overexpression. Culture supernatants were collected at 0, 24, 48, 72, 96, and 120 hpi, and CA levels were measured using an ELISA kit. (G) Virus titer determination upon eEF1A overexpression. Virus titers in culture supernatants were determined at 72 hpi using the Reed-Muench method. (H) Immunofluorescence analysis of gp37 expression upon eEF1A overexpression. At 72 hpi, cells were fixed and stained with an anti-gp37 antibody. Representative images are shown (20× magnification). All experiments were performed at least three times, and representative results are shown. Data are presented as mean ± SD from an experiment performed in triplicate. Statistical significance was determined using unpaired two-tailed Student's *t*-tests. *$P < 0.05$, **$P < 0.01$, and ***$P < 0.001$.

at 24 and 48 hpi, whereas a significant reduction was observed at 72, 96, and 120 hpi (Fig. 1B). Consistent with these findings, the viral titer was 51-fold lower than that of the si-NC control group at 72 hpi (Fig. 1C). Furthermore, IFA results also indicated a significant reduction in the fluorescence intensity labeled by the gp37 antibody following si-eEF1A treatment, indicating reduced viral antigen expression (Fig. 1D). Conversely, in eEF1A-overexpressing cells, Western blot analysis showed that the viral transmembrane protein gp37 remained comparable to the empty vector (EV) control group at 48 hpi, whereas a markedly increased level was observed at 72 hpi (Fig. 1E and Fig. S1D). Measurement of viral particles in the culture supernatant revealed that ALV-J CA secretion was comparable between eEF1A-overexpressing and control cells at 24 and 48 hpi but was significantly elevated at 72, 96, and 120 hpi (Fig. 1F). The ALV-J titer increased by 30-fold at 72 hpi compared to EV-transfected cells (Fig. 1G). Furthermore, upon eEF1A overexpression, IFA revealed a substantial increase in the gp37-specific fluorescence signal, suggesting enhanced viral antigen expression (Fig. 1H). Collectively, these results demonstrate that the host protein eEF1A positively regulates the replication ability of ALV-J. Moreover, this discrepancy between moderately altered CA levels and large-magnitude changes in the infectious titer suggests that eEF1A knockdown may reduce the specific infectivity of assembled virions rather than merely decreasing total particle production.

eEF1A associates with ALV-J reverse transcriptase

Having established that eEF1A is a critical regulator of ALV-J replication, we next sought to delineate the specific stage of the viral life cycle in which eEF1A exerts its function. To this end, we first examined the potential interactions between eEF1A and various ALV-J proteins, including protease (PR), matrix protein (MA), capsid protein (CA), integrase (IN), reverse transcriptase (RT), transmembrane protein (TM), and surface glycoprotein (SU). Co-immunoprecipitation assays revealed that eEF1A associates with the viral RT, IN, and PR, with the most robust association observed for RT (Fig. 2A). Thus, we further examined the association between eEF1A and RT using confocal microscopy, which showed clear colocalization of the two proteins predominantly in the cytoplasmic and perinuclear regions (Fig. 2B). To validate this interaction under physiological infection conditions, we performed co-IP assays in ALV-J-infected DF-1 cells, which consistently demonstrated an association between endogenous eEF1A and ALV-J RT (Fig. 2C). Moreover, we isolated RTC from ALV-J-infected cells using sucrose gradient centrifugation. The gradient was fractionated from bottom to top, and each fraction was analyzed by Western blotting. The results showed that eEF1A was detected in fractions that also contained viral RT, and their abundance showed a strong positive correlation, indicating a specific association (Fig. 2D). Collectively, our findings demonstrate a robust association between eEF1A and ALV-J RT. Because RT is the core catalytic enzyme of reverse transcription, the present study focuses on the eEF1A-RT association; the potential functional roles of the eEF1A-IN and eEF1A-PR associations are considered in the Discussion.

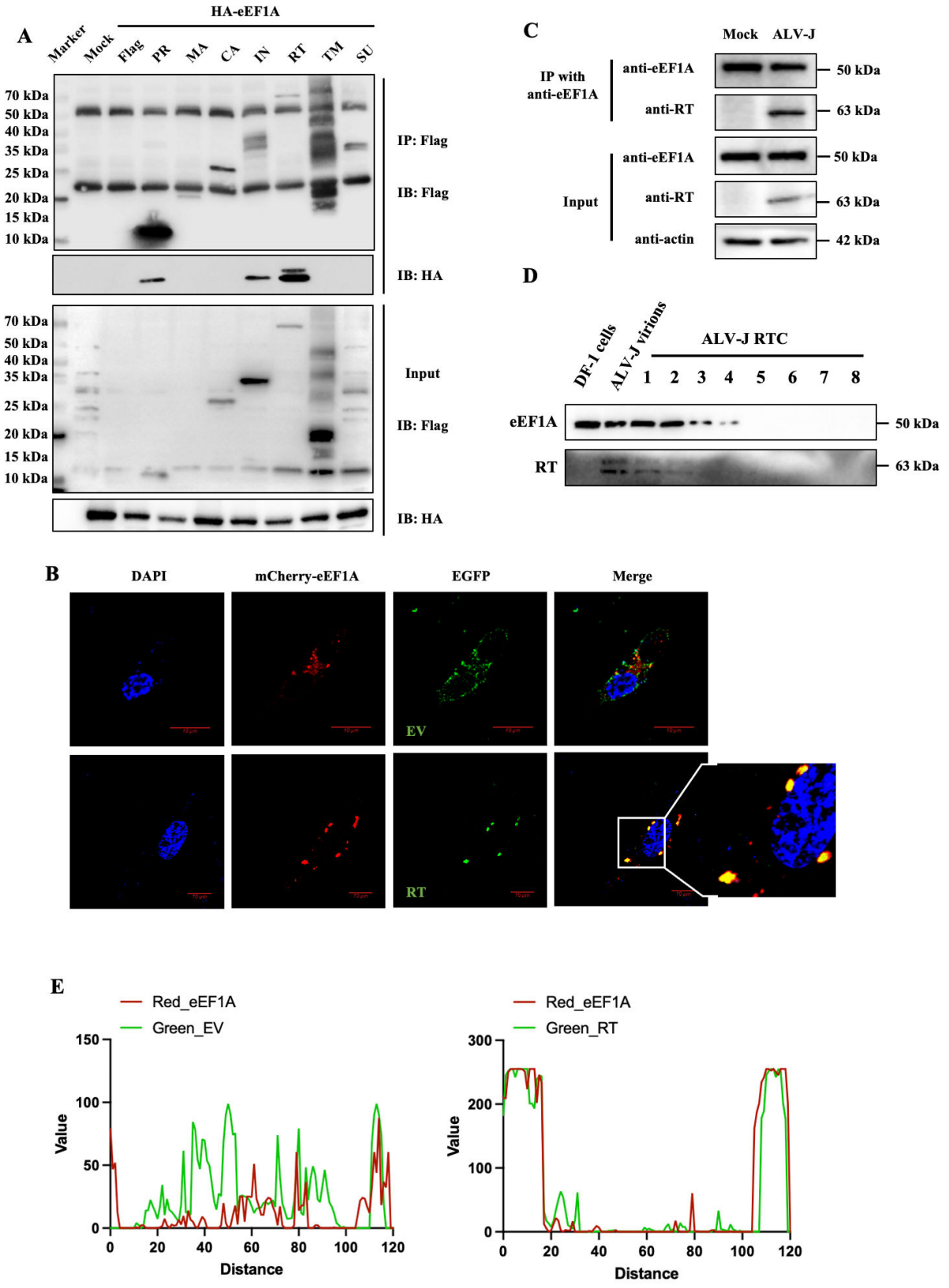

FIG 2 eEF1A associates with ALV-J reverse transcriptase. (A) Co-IP analysis of eEF1A interaction with viral proteins. DF-1 cells were co-transfected with HA-tagged eEF1A and Flag-tagged ALV-J protein expression plasmids (PR, MA, CA, IN, RT, TM, and SU), as indicated. At 48 hpi, cell lysates were immunoprecipitated with anti-Flag antibody, followed by Western blotting with anti-Flag and anti-HA antibodies. Immunoglobulin heavy-chain (~50 kDa) and light-chain (~25 kDa) bands

(Continued on next page)

Fig 2 (Continued)

are indicated where visible in immunoprecipitation panels. (B) Colocalization analysis of eEF1A and ALV-J RT. DF-1 cells were co-transfected with EGFP-RT (green) and mCherry-eEF1A (red) expression plasmids. At 48 h post-transfection, cells were fixed, and nuclei were stained with DAPI (blue). Colocalization was analyzed by confocal microscopy. EV served as a negative control. Scale bars, 10 µm. (C) Co-IP analysis of endogenous eEF1A with viral proteins. DF-1 cells were infected with ALV-J at an MOI of 0.01. At 48 hpi, cell lysates were immunoprecipitated with anti-eEF1A antibody, followed by Western blotting with the indicated antibodies. (D) Association of eEF1A with viral RTCs. DF-1 cells were infected with ALV-J at an MOI of 0.01. At 8 hpi, RTCs were isolated from infected cells. RTC lysates were analyzed by Western blotting with anti-eEF1A and anti-RT antibodies. Total DF-1 cell lysate and purified ALV-J virions were used as controls. (E) Colocalization coefficient analysis. Image preprocessing was performed in Leica TCS SP8 STED 3×. The regions of interest were defined, and the two fluorescence channels were split for individual analysis. Object-based colocalization analysis was performed to calculate the colocalization coefficients. The percentage of objects in Channel eEF1A that colocalized with at least one object from Channel RT was identified. All experiments were performed at least three times, and representative results are shown.

eEF1A promotes ALV-J reverse transcription efficiency

Next, we investigated whether eEF1A influences the critical reverse transcription step of the ALV-J life cycle via its association with viral RT. To assess this, we first measured the synthesis of viral late reverse transcription products and early DNA copies in eEF1A-manipulated cells using qPCR. Analysis of reverse transcription products revealed that eEF1A depletion significantly reduced the synthesis of late viral DNA copies, with a reduction of approximately 60% compared to the control group (Fig. 3A), while early DNA synthesis remained largely unaffected (Fig. 3B). This resulted in a greater than 50% decrease in the overall reverse transcription efficiency compared to si-NC control (Fig. 3C). Conversely, eEF1A overexpression significantly enhanced late DNA synthesis by nearly 80% compared to the EV control group (Fig. 3A), whereas early viral DNA synthesis showed no substantial change (Fig. 3B). Accordingly, reverse transcription efficiency was increased approximately twofold in eEF1A-overexpressing cells relative to the EV control (Fig. 3D). As with reverse transcription efficiency, the RT assay indicated that si-eEF1A treatment had a significantly lower total RT-assay signal than the si-NC control. Moreover, the RT-assay signal of the si-NC control group reached a peak of 25.45 ng/mL at 96 hpi, whereas the peak of the si-eEF1A treatment group was only 16.5 ng/mL (Fig. 3E). In contrast, overexpression of eEF1A significantly enhanced the RT-assay signal compared with the EV control group. The RT-assay signal of the eEF1A overexpression group reached a peak of approximately 31.33 ng/mL, which is approximately 1.3-fold higher than that of the EV control group (23.67 ng/mL) (Fig. 3F). Further analysis of RTCs isolated from siRNA-treated cells showed a markedly reduced RT level in sedimented fractions 1–3 when eEF1A expression was downregulated (Fig. 3G). Correspondingly, viral DNA levels in these fractions were also significantly decreased (Fig. 3H). These results indicate that the host protein eEF1A plays a key role in ALV-J reverse transcription.

Molecular determinants of the eEF1A-RT interaction

Based on the above results, we hypothesized that the host protein eEF1A regulates viral replication by associating with the RT and modulating the efficiency of reverse transcription. To verify this hypothesis, we first sought to characterize the molecular basis of the eEF1A-RT interaction and then to validate the changes in viral reverse transcription and replication by disrupting the eEF1A-RT interaction. We performed homology modeling and molecular docking to characterize the eEF1A-RT interaction. The docking results revealed the formation of 20 hydrogen bonds and six salt bridge interactions between eEF1A and ALV-J RT (Table S2). The predicted model revealed an extensive interaction interface, with eEF1A domain I (amino acids 17–56 and 120–135) engaging the thumb and connection subdomains of RT (amino acids 245–395) (Fig. S2).

To map the precise region within eEF1A required for interaction with ALV-J RT, we generated a series of N-terminal HA-tagged truncation and deletion mutants (Fig. 4A). Co-IP assays revealed that deletion of Domain I markedly impaired the association with RT (Fig. 4B), consistent with molecular docking predictions (Fig. S2). Among three targeted internal deletion mutants—1–56 del, 120–135 del, and 1–135 del—only

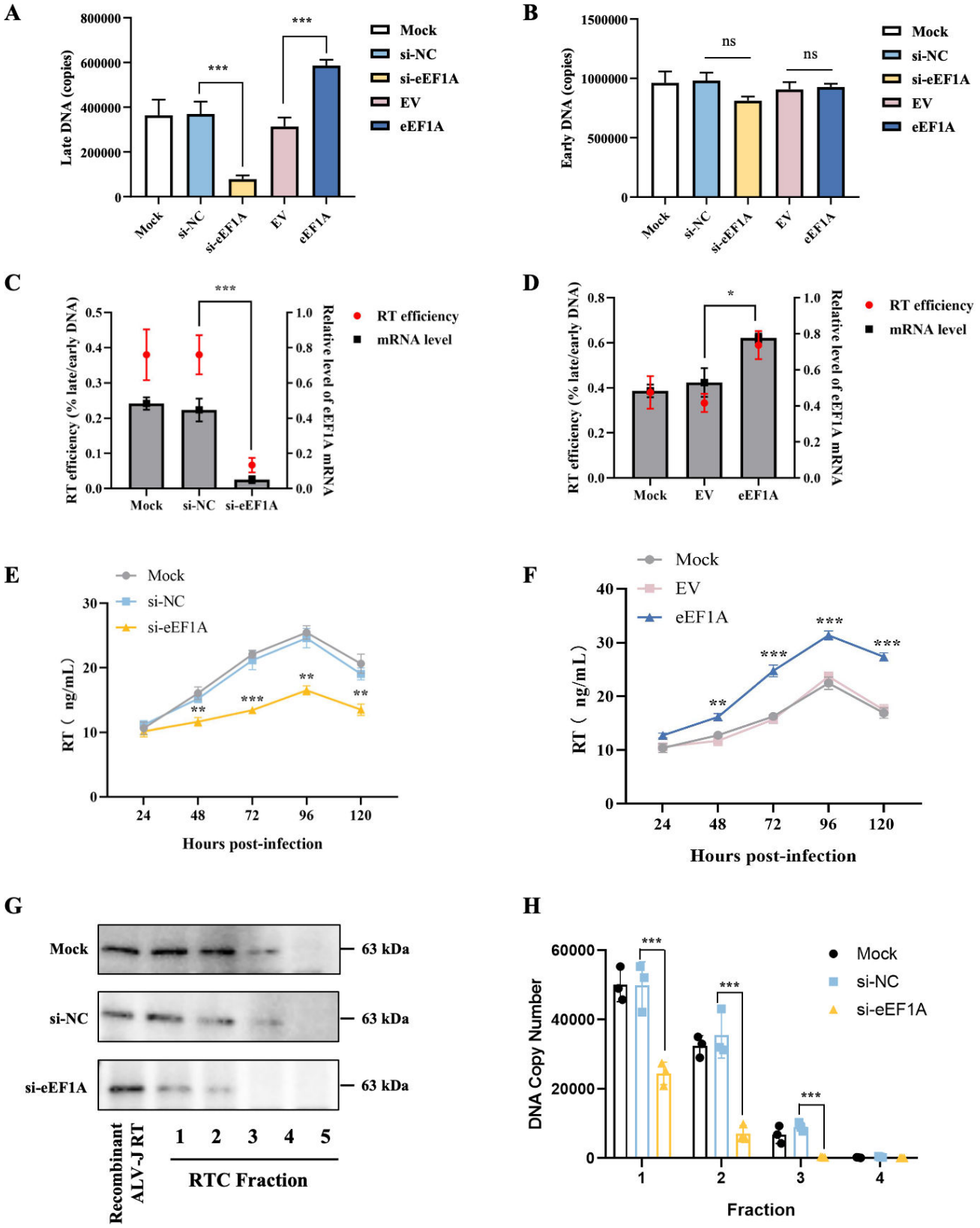

FIG 3 eEF1A promotes ALV-J reverse transcription efficiency. (A) qPCR analysis of late viral DNA synthesis. DF-1 cells were transfected with siRNA targeting eEF1A or eEF1A overexpression plasmids, along with si-NC or EV as negative controls, respectively. At 24 h post-transfection, cells were infected with ALV-J at an MOI of 0.01. Total cytoplasmic DNA was collected at 8 h post-infection, and the levels of late viral DNA copies were quantified by qPCR. (B) qPCR analysis of early

(Continued on next page)

Fig 3 (Continued)

viral DNA synthesis. Experimental procedures were performed as described in panel A. Early viral DNA copies were quantified by qPCR. (C) Reverse transcription efficiency upon eEF1A depletion. Reverse transcription efficiency was calculated as the ratio of late to early viral DNA copies, expressed as a percentage. Data are shown for cells transfected with siRNA targeting eEF1A compared to si-NC control. (D) Reverse transcription efficiency upon eEF1A overexpression. Reverse transcription efficiency was calculated as the ratio of late to early viral DNA copies, expressed as a percentage. Data are shown for cells transfected with eEF1A overexpression plasmids compared to empty vector (EV) control. (E) RT-assay signal upon eEF1A depletion. DF-1 cells were transfected with si-eEF1A or si-NC and infected with ALV-J (MOI = 0.01) at 24 h post-transfection. Cells were harvested at 24, 48, 72, 96, and 120 hpi, and the RT-assay signal was quantified using a colorimetric reverse transcriptase assay. (F) RT-assay signal upon eEF1A overexpression. DF-1 cells were transfected with HA-eEF1A overexpression plasmids or EV and infected with ALV-J (MOI = 0.01) at 24 h post-transfection. Cells were harvested at 24, 48, 72, 96, and 120 hpi, and RT activity was quantified using a colorimetric reverse transcriptase assay. (G) Western blot analysis of viral RT in isolated RTCs. DF-1 cells were transfected with siRNA targeting eEF1A or si-NC and infected with ALV-J at 24 h post-transfection. At 8 hpi, RTCs were isolated, and protein expression was detected by Western blotting using an anti-RT antibody. (H) qPCR analysis of viral DNA in isolated RTCs. DF-1 cells were transfected with siRNA targeting eEF1A or si-NC and infected with ALV-J at 24 h post-transfection. At 8 hpi, RTCs were isolated, and viral DNA copies were quantified by qPCR. Data are presented as mean ± SD from an experiment performed in triplicate. Statistical significance was determined using unpaired two-tailed Student's *t*-tests. *$P < 0.05$, **$P < 0.01$, and ***$P < 0.001$.

removal of residues 120–135 within Domain I completely abolished the interaction with RT, identifying this region as essential (Fig. 4C and D). To further refine the interaction interface, we introduced overlapping double-alanine substitutions across the 120–135 segment. Mutants 124-125AA, 128-129AA, and 134-135AA each significantly reduced the association with RT (Fig. 4E). Individual mutations at E124, K129, or R134 to alanine each partially reduced the association with RT, but the combined triple mutation (E124A/K129A/R134A, termed "EKR") almost completely abolished the interaction, showing an additive effect (Fig. 4F). Confocal microscopy analysis revealed pronounced colocalization between eEF1A and RT. In contrast, this colocalization was markedly weakened upon single-residue mutations (E124A, K129A, and R134A), as well as the triple mutation (EKR) of eEF1A (Fig. 4G). To quantitatively assess these observations, we performed fluorescence intensity profiling using ImageJ. Along the indicated linescan, wild-type eEF1A exhibited fluorescence intensity peaks that closely aligned with those of RT, indicating robust colocalization. However, for the EKR triple mutant, the fluorescence peaks almost complete loss of peak overlap, with minimal alignment between eEF1A and RT signals (Fig. 4H). These results indicate that residues E124, K129, and R134 in domain I of eEF1A are required for efficient association with ALV-J RT under the assay conditions used.

Similarly, to identify the key functional residues within ALV-J RT that mediate its interaction with eEF1A, we generated a series of truncated RT mutants (Fig. 5A). Co-IP assays demonstrated reduced association when the thumb domain was deleted and almost no association when both the thumb and connection domains were removed (Fig. 5B). To further dissect the role of the thumb domain, a series of alanine substitution mutations were introduced into RT, creating 15 non-overlapping mutations with five consecutive alanine residues covering the thumb domain (Fig. 5C). Among these, mutations spanning residues 250–254 significantly disrupted the RT-eEF1A association (Fig. 5D). To refine these findings, overlapping double-alanine substitutions were introduced, generating four new mutant RT constructs: 250-251AA, 251-252AA, 252-253AA, and 253-254AA. Among these, Co-IP analysis revealed that the 250-251AA mutation particularly impaired the interaction (Fig. 5E). Subsequent single-alanine substitutions confirmed that the W250A mutation dramatically impaired the RT-eEF1A association, while the D251A mutation showed a negligible effect (Fig. 5F). Confocal microscopy analysis revealed pronounced colocalization between RT and eEF1A, as evidenced by the substantial overlap of green (RT) and red (eEF1A) fluorescence signals (Fig. 5G). In contrast, this colocalization was markedly weakened upon the W250A mutation, whereas the D251A mutation showed only a minor impact (Fig. 5G). Fluorescence intensity profiling along the indicated lines revealed that wild-type RT exhibited intensity peaks that closely aligned with those of eEF1A, indicating robust colocalization. However, for the W250A mutant, the fluorescence peaks showed substantial separation, reflecting markedly reduced colocalization. In contrast, the D251A mutant retained

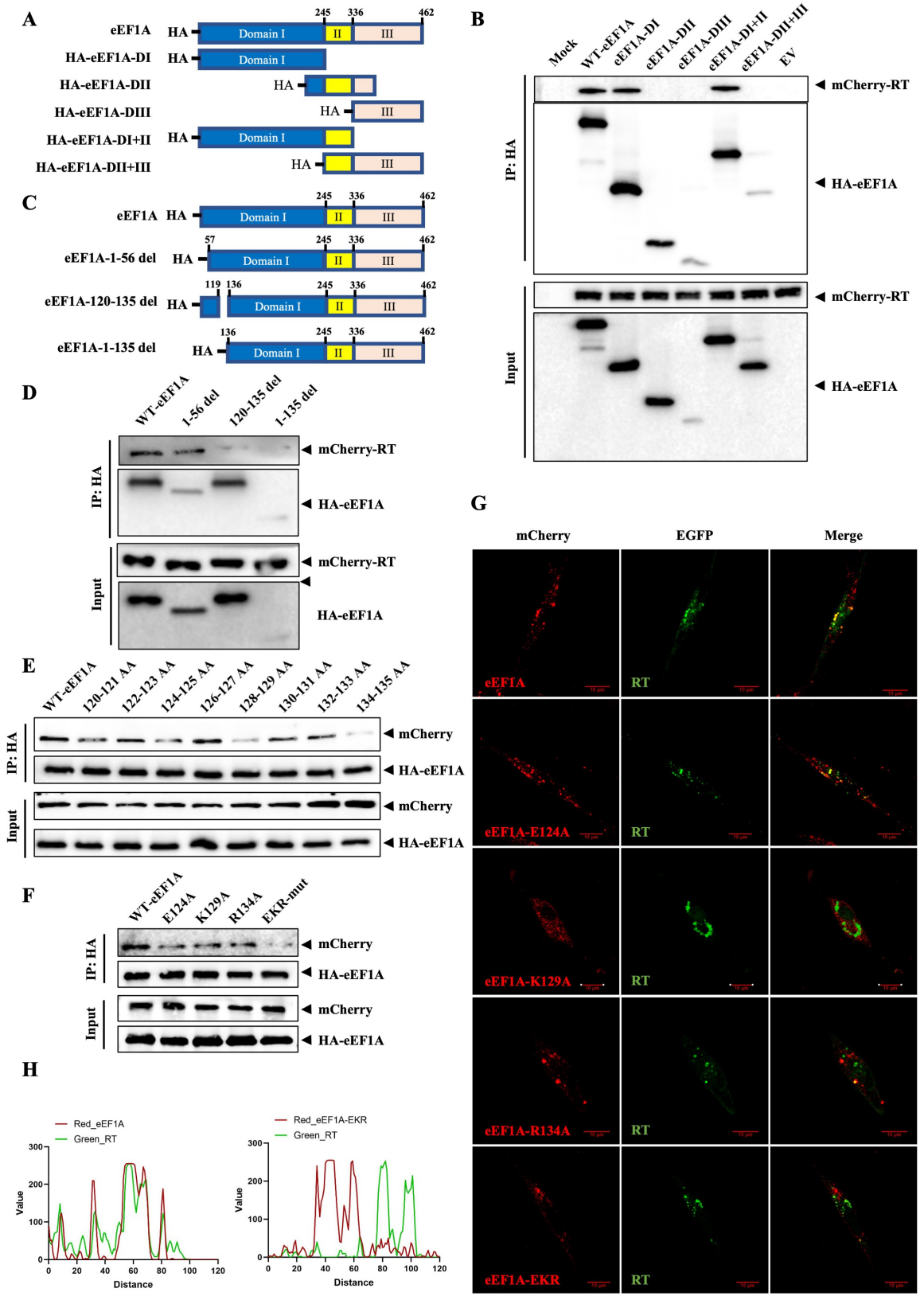

FIG 4 Residues E124, K129, and R134 in eEF1A domain I mediate interaction with ALV-J RT. (A) Schematic diagram of eEF1A truncation and deletion mutants. Schematic representation of HA-tagged eEF1A truncation mutants and domain deletion mutants. Domain boundaries are indicated according to the eEF1A domain architecture. (B) Co-IP analysis of RT binding to eEF1A truncation mutants. DF-1 cells were co-transfected with mCherry-RT and HA-tagged WT-eEF1A

(Continued on next page)

Fig 4 (Continued)

or the indicated truncation mutants. At 48 h post-transfection, cell lysates were immunoprecipitated with anti-HA antibody, followed by western blotting with anti-mCherry and anti-HA antibodies. (C) Schematic diagram of internal deletion mutants within eEF1A domain I. Schematic representation of HA-tagged eEF1A domain I internal deletion mutants. The deleted amino acid regions are indicated. (D) Co-IP analysis of RT binding to eEF1A domain I internal deletion mutants. DF-1 cells were co-transfected with mCherry-RT and HA-tagged eEF1A domain I internal deletion mutants. At 48 h post-transfection, cell lysates were immunoprecipitated with anti-HA antibody, followed by western blotting with anti-mCherry and anti-HA antibodies. (E) Co-IP analysis of RT binding to eEF1A double-alanine mutants. DF-1 cells were co-transfected with mCherry-RT and HA-tagged wild-type eEF1A or the indicated double-alanine mutants. At 48 h post-transfection, cell lysates were immunoprecipitated with anti-HA antibody, followed by western blotting with anti-mCherry and anti-HA antibodies. (F) Co-IP analysis of RT binding to eEF1A single- and triple-alanine mutants. DF-1 cells were co-transfected with mCherry-RT and HA-tagged wild-type eEF1A, single-residue mutants (E124A, K129A, R134A), or the triple mutant (EKR). At 48 hpi, cell lysates were immunoprecipitated with anti-HA antibody, followed by western blotting with anti-mCherry and anti-HA antibodies. (G) Confocal microscopy analysis of co-localization between eEF1A mutants and RT. DF-1 cells were co-transfected with EGFP-RT and mCherry-tagged wild-type eEF1A or the indicated eEF1A mutants (E124A, K129A, R134A, and EKR). At 48 h post-transfection, cells were fixed, and nuclei were stained with DAPI. Co-localization was analyzed by confocal microscopy (Leica TCS SP8 STED 3X). Scale bars, 10 µm. (H) Fluorescence intensity distribution analysis. Fluorescence intensity profiles along the indicated lines were generated using ImageJ software. Green (EGFP-RT) and red (mCherry-eEF1A) fluorescence intensities are plotted as a function of distance. Representative profiles from three independent experiments are shown. All experiments were performed at least three times and representative results are shown.

considerable peak overlap, consistent with its preserved association (Fig. 5H). Structural analysis indicated that the aromatic side chain of W250 is buried within the hydrophobic core of RT and forms key interactions with neighboring residues, including T248, D251, K254, and P285 (Fig. 5I). While molecular docking predicts a general binding interface between eEF1A domain I and the RT thumb domain, it does not unambiguously resolve a direct E124/K129/R134–W250 side-chain pairing. Instead, our proposed model of the EKR residues engaging the W250-centered hydrophobic interface is inferred primarily from our mutagenesis and functional data, which convergently identify these residues as the critical functional determinants of the interaction (Fig. 5J). These results indicate that W250 serves as a critical structural determinant mediating the interaction between RT and eEF1A. We acknowledge that alanine substitutions could, in principle, alter co-immunoprecipitation signals indirectly through effects on protein folding, stability, solubility, aggregation, or antibody accessibility. However, the concordant loss of eEF1A binding and the functional defects in reverse transcription and viral replication observed with the W250A mutant infectious clone, together with molecular docking predictions supporting a direct contact interface, strongly support a specific role for W250 in mediating the eEF1A-RT interaction. Overall, the above results have revealed the molecular determinants of the association between eEF1A and ALV-J RT. Specifically, the E124, K129, and R134 residues in the Domain I of eEF1A and the W250 residue in the thumb domain of RT, respectively, play roles in mediating the interaction between the two proteins.

Mutations in residues E124, K129, and R134 of eEF1A impair the reverse transcription efficiency and replication capacity of ALV-J

Next, to directly assess the functional impact of disrupting the eEF1A-RT interaction, we first attempted to generate complete eEF1A knockout DF-1 cells using CRISPR-Cas9. Although HI-TOM sequencing analysis confirmed successful gene editing at the target locus (Fig. 6A), no stable knockout cell line could be established as edited cells exhibited severe proliferation defects and underwent rapid cell death within three passages. We, therefore, established a stable eEF1A-knockdown cell line (eEF1A-KD) using lentivirus-delivered shRNA, which achieved over 70% reduction in eEF1A expression without affecting cell viability. eEF1A-KD cells were subsequently complemented with either wild-type eEF1A or the EKR triple-mutant eEF1A (eEF1A-EKRmut) and infected with ALV-J. Cells were harvested at the indicated time points for subsequent analyses.

In eEF1A-KD cells, complementation with wild-type eEF1A fully restored ALV-J late DNA synthesis and reverse transcription efficiency to levels comparable to those observed in wild-type DF-1 cells (Fig. 6B through D). In contrast, complementation

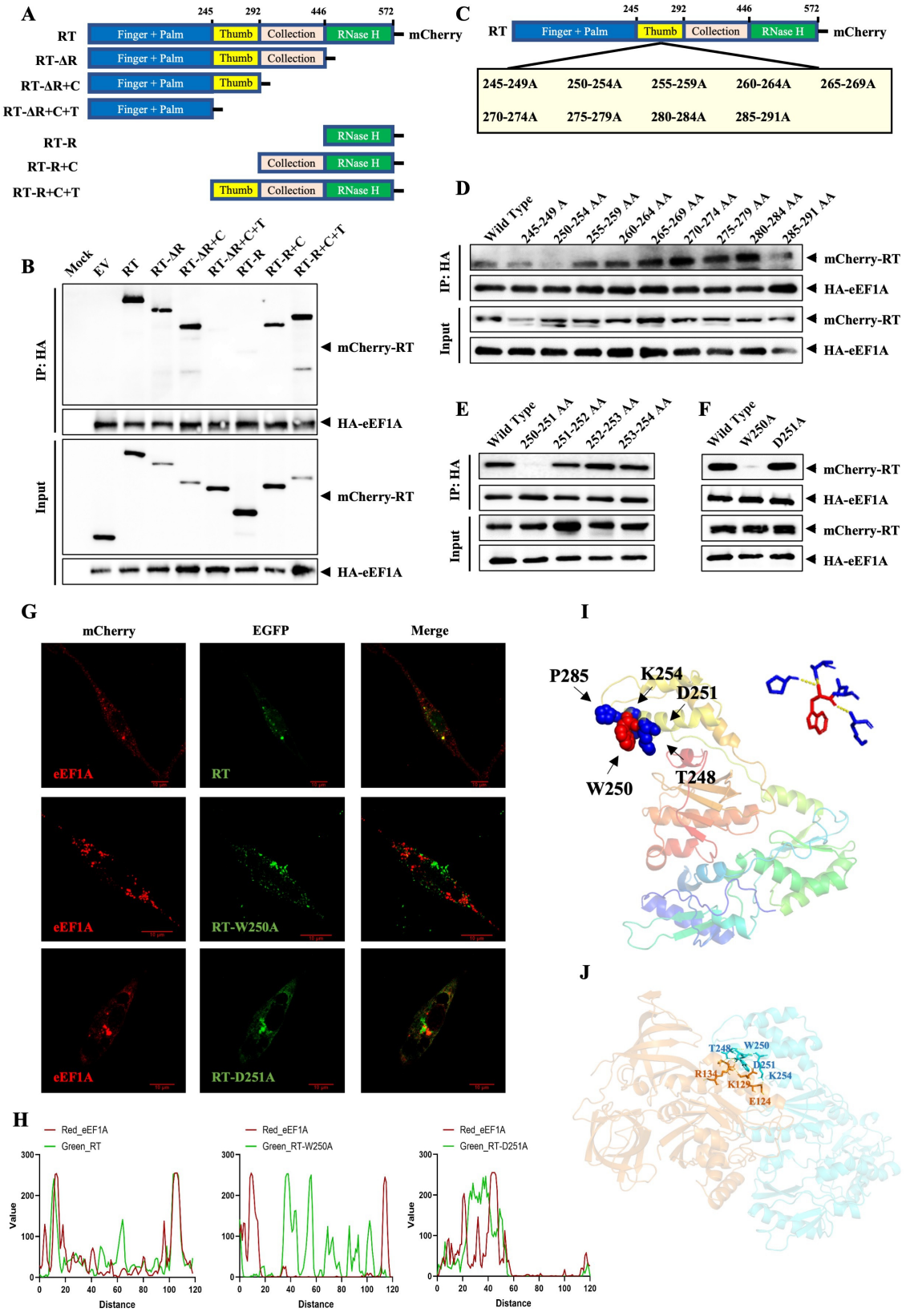

FIG 5 Residue W250 in ALV-J RT defines the eEF1A-binding interface. (A) Schematic diagram of RT truncation mutants. Schematic representation of ALV-J RT truncation mutants. Domain boundaries are indicated according to the RT domain architecture. (B) Co-IP analysis of eEF1A binding to RT truncation mutants. DF-1 cells were co-transfected with HA-tagged eEF1A and the indicated Flag-tagged RT truncation mutants. At 48 h post-transfection, cell lysates were

(Continued on next page)

Fig 5 (Continued)

immunoprecipitated with anti-Flag antibody, followed by western blotting with anti-HA and anti-Flag antibodies. (C) Schematic diagram of alanine-scanning mutants within the RT thumb domain. Schematic representation of 15 non-overlapping alanine substitution mutants covering the thumb domain of ALV-J RT. Each mutant contains five consecutive alanine residues. (D) Co-IP analysis of eEF1A binding to RT alanine-scanning mutants. DF-1 cells were co-transfected with HA-tagged eEF1A and the indicated Flag-tagged RT alanine-scanning mutants. At 48 h post-transfection, cell lysates were immunoprecipitated with anti-Flag antibody, followed by western blotting with anti-HA and anti-Flag antibodies. (E) Co-IP analysis of eEF1A binding to RT double-alanine mutants. DF-1 cells were co-transfected with HA-tagged eEF1A and Flag-tagged wild-type RT or the indicated double-alanine mutants (250-251AA, 251-252AA, 252-253AA, and 253-254AA). At 48 hpi, cell lysates were immunoprecipitated with anti-Flag antibody, followed by western blotting with anti-HA and anti-Flag antibodies. (F) Co-IP analysis of eEF1A binding to RT single-alanine mutants. DF-1 cells were co-transfected with HA-tagged eEF1A and Flag-tagged wild-type RT or the indicated single-alanine mutants (W250A and D251A). At 48 h post-transfection, cell lysates were immunoprecipitated with anti-Flag antibody, followed by western blotting with anti-HA and anti-Flag antibodies. (G) Confocal microscopy analysis of co-localization between RT mutants and eEF1A. DF-1 cells were co-transfected with mCherry-eEF1A and EGFP-tagged wild-type RT, W250A mutant, or D251A mutant. At 48 h post-transfection, cells were fixed, and nuclei were stained with DAPI. Co-localization was analyzed by confocal microscopy (Leica TCS SP8 STED 3X). Scale bars, 10 µm. (H) Fluorescence intensity distribution analysis of co-localization between RT mutants and eEF1A. Fluorescence intensity profiles along the indicated lines were generated using ImageJ software. Green (EGFP-RT) and red (mCherry-eEF1A) fluorescence intensities are plotted as a function of distance along the linescan. Representative profiles from three independent experiments are shown. (I) Schematic diagram of the predicted RT structure. The predicted model shows that W250 engages with other hydrophobic amino acids, providing a spatially proximal region supported by hydrophobic interactions. (J) Schematic diagram of the proposed interaction model. The model illustrates that residues E124, K129, and R134 of eEF1A interact with the hydrophobic interface formed by RT-W250. Western blots and immunofluorescence images are representative of at least three independent experiments with consistent results.

with the eEF1A-EKRmut failed to rescue these defects, resulting in significantly reduced late DNA synthesis and reverse transcription efficiency compared with the wild-type eEF1A complementation group (Fig. 6B through D). RT-assay signal measurements showed that re-expression of wild-type eEF1A in eEF1A-KD cells completely restored the ALV-J RT-assay signal, whereas complementation with eEF1A-EKRmut led to a marked reduction in the RT-assay signal relative to wild-type DF-1 cells (Fig. 6E). Measurement of viral capsid antigen (CA) levels in the culture supernatants by ELISA further confirmed this trend as CA protein levels increased progressively over time in the wild-type eEF1A complementation group but remained substantially lower in the eEF1A-EKRmut group. (Fig. 6F). Moreover, qPCR analysis of intracellular viral genome copies revealed that wild-type eEF1A complementation significantly increased viral copy numbers, whereas eEF1A-EKRmut only partially restored or failed to restore viral genome accumulation (Fig. 6G). These findings were further supported by Western blot analysis, which demonstrated substantially lower levels of viral protein gp37 expression in cells complemented with eEF1A-EKRmut compared with those expressing wild-type eEF1A (Fig. 6H). Taken together, these results demonstrate that residues E124, K129, and R134 in eEF1A are essential for efficient ALV-J reverse transcription and subsequent viral replication.

Residue W250 in the RT thumb domain is essential for ALV-J reverse transcription and replication

Given that eEF1A associates with viral RT, we next investigated whether key residues within RT contribute to efficient reverse transcription and viral replication. To this end, an infectious clone carrying a W250A substitution in RT (rALV-J-W250A) was generated. Western blot analysis of the RT-reactive species detected no significant difference between rALV-J and rALV-J-W250A (Fig. 7A). The IFA results also indicated that DF-1 cells inoculated with rALV-J-W250A showed specific green fluorescence but reduced viral antigen signals compared to the rALV-J group at 72 hpi (Fig. 7B).

To directly assess the impact of the W250 mutation on the reverse transcription process, intracellular viral DNA intermediates were quantified. qPCR analysis showed that the late DNA copy numbers were significantly reduced in cells infected with the rALV-J-W250A compared with those infected with rALV-J (Fig. 7C). Accordingly, calculation of reverse transcription efficiency revealed a marked decrease in the rALV-J-W250A group, indicating that substitution of W250 severely compromises the efficiency of viral reverse transcription (Fig. 7D). RT assays demonstrated that the

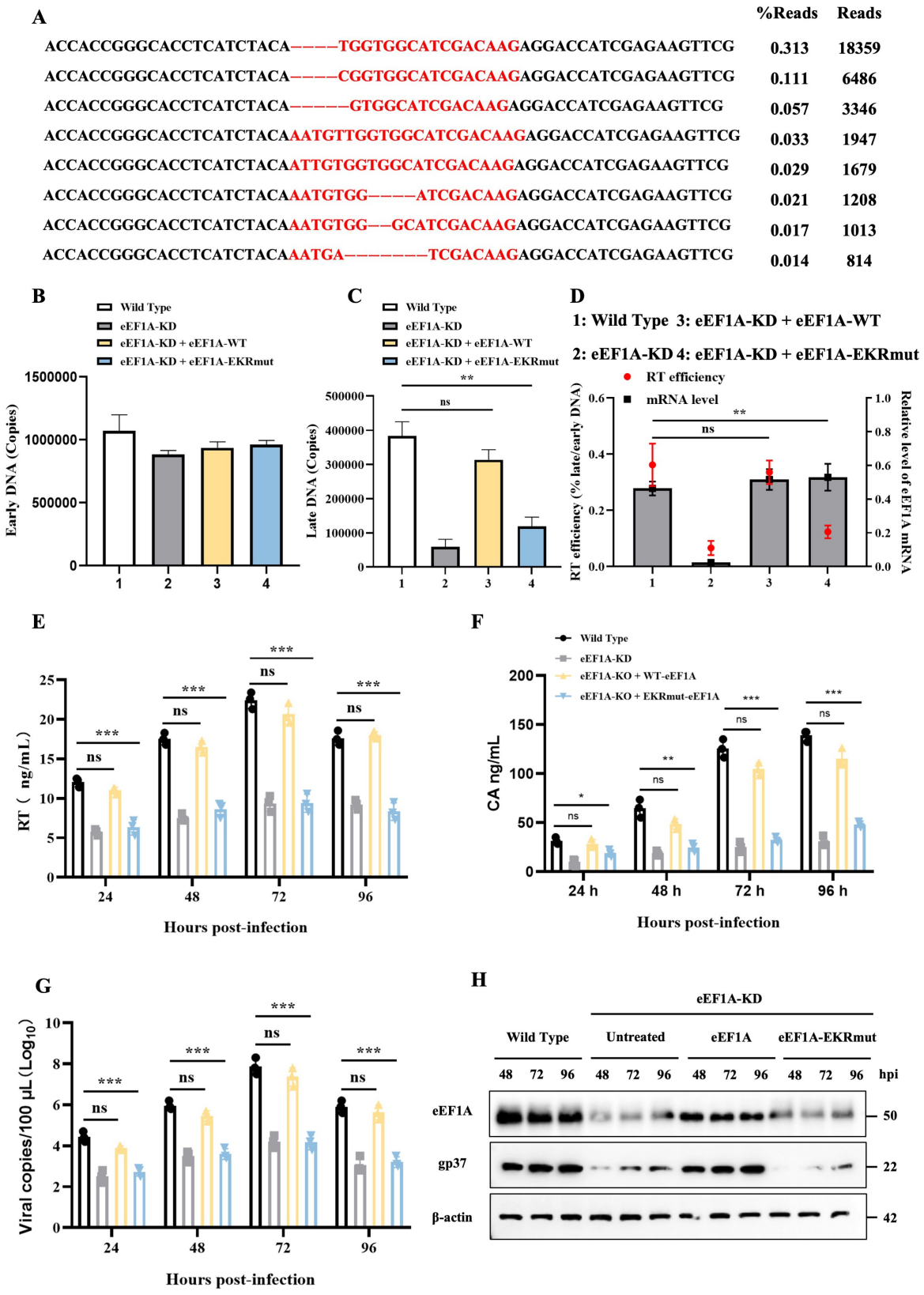

FIG 6 Residues E124, K129, and R134 in eEF1A are essential for ALV-J reverse transcription and replication. (A) Sequencing analysis of eEF1A editing. Sequencing analysis of eEF1A editing. HI-TOM sequencing analysis of the eEF1A target locus (exon 2) in CRISPR-Cas9-edited DF-1 cells after puromycin selection. The average sequencing depth was ~ 2,000 ×, with approximately 2.9% of reads representing residual wild-type alleles. Representative editing outcomes and their read

(Continued on next page)

Fig 6 (Continued)

counts are shown. (B and C) qPCR analysis of viral DNA synthesis. DF-1 cells were transduced with lentivirus-delivered shRNA to establish a stable eEF1A-KD cell line. eEF1A-KD cells were subsequently transfected with eEF1A-WT or eEF1A-EKRmut, followed by infection with ALV-J at an MOI of 0.01 at 24 h post-transfection. Normal DF-1 cells were included as a control. Total cellular DNA was collected at 8 hpi. Early (B) and late (C) viral DNA copies were quantified by qPCR. (D) Reverse transcription efficiency. Reverse transcription efficiency was calculated as the ratio of late to early viral DNA copies, expressed as a percentage (red dots, left Y-axis). eEF1A protein levels are shown as histogram bars (right Y-axis). Significance indicators refer to statistical differences in reverse transcription efficiency between groups. (E) RT-assay signal. Cells were harvested at 24, 48, 72, and 96 hpi, and the RT-assay signal was quantified using a colorimetric reverse transcriptase assay. (F) ELISA analysis of viral CA secretion. Culture supernatants were collected at 24, 48, 72, and 96 hpi, and CA levels were measured by ELISA. (G) qPCR analysis of viral genome copies. Cells were harvested at 24, 48, 72, and 96 hpi, and intracellular viral genome copies were quantified by qPCR. (H) Western blot analysis of viral protein expression. Cell lysates were collected at 48 hpi, and protein expression was detected using anti-eEF1A and anti-gp37 antibodies. Western blot images are representative of at least three independent experiments with consistent results. Quantitative data are presented as mean ± SD from three independent biological replicates, each assayed in technical triplicate. Statistical significance was determined using unpaired two-tailed Student's *t*-tests. **P* < 0.05, ***P* < 0.01, and ****P* < 0.001, while "ns" indicates non-significance.

RT-assay signal of the rALV-J-W250A was significantly lower than that of the rALV-J (Fig. 7E). In parallel, ELISA analysis of viral CA antigen levels in culture supernatants revealed substantially reduced CA production in cells infected with the rALV-J-W250A at 24, 48, 72, and 96 hpi (Fig. 7F). Consistently, qPCR analysis showed that viral copy numbers were markedly decreased in the rALV-J-W250A group (Fig. 7G). Western blot analysis further confirmed reduced expression of viral gp37 proteins in cells infected with the rALV-J-W250A compared with rALV-J (Fig. 7H). Taken together, these results demonstrate that tryptophan 250 in the RT thumb domain is critical for efficient reverse transcription and productive replication of ALV-J, providing complementary evidence that RT function is required for eEF1A-mediated regulation of the viral reverse transcription process.

The eEF1A–RT interaction is conserved across multiple ALV subgroups

Given that eEF1A regulates ALV-J reverse transcription and viral replication through association with RT, we next investigated whether this regulatory mechanism is conserved among other major ALV subgroups. To this end, the effects of eEF1A on the replication of ALV-A, ALV-B, and ALV-K were systematically examined. We first assessed the impact of eEF1A depletion on viral replication. DF-1 cells with stable eEF1A knockdown were infected with ALV-A, ALV-B, or ALV-K, and viral replication was evaluated by measuring CA levels in culture supernatants. ELISA results showed that knockdown of eEF1A led to a significant reduction in CA production for all three ALV subgroups, indicating that eEF1A is required for efficient replication of ALV-A, ALV-B, and ALV-K (Fig. 8A through C). Conversely, DF-1 cells transiently overexpressing eEF1A were infected with ALV-A, ALV-B, or ALV-K, followed by ELISA-based quantification of CA levels. Overexpression of eEF1A resulted in a marked increase in CA production for all three subgroups compared with control cells, demonstrating that elevated eEF1A levels promote the replication of ALV-A, ALV-B, and ALV-K (Fig. 8D through F).

To determine whether the effect of eEF1A on different ALV subgroups involves an association with RT, Co-IP assays were performed. The results revealed that eEF1A associated with RT proteins from ALV-A, ALV-B, and ALV-K, indicating that the eEF1A-RT interaction is conserved across all four ALV subgroups examined (Fig. 8G). Consistent with this observation, sequence alignment analysis of RT proteins from different ALV subgroups revealed that this region of RT, including the tryptophan residue corresponding to W250, is conserved across the subgroups examined (Fig. 8H), consistent with a shared functional dependence on eEF1A. Finally, to assess the functional relevance of the EKR residues of eEF1A in the replication of different ALV subgroups, eEF1A-knockdown DF-1 cells were complemented with either wild-type eEF1A or the EKR-mutant eEF1A, followed by infection with ALV-A, ALV-B, or ALV-K. Complementation with wild-type eEF1A effectively restored the replication of all three ALV subgroups, whereas complementation with the EKR-mutant eEF1A failed to rescue viral replication and resulted in significantly reduced CA production (Fig. 8I through K). These results demonstrate that

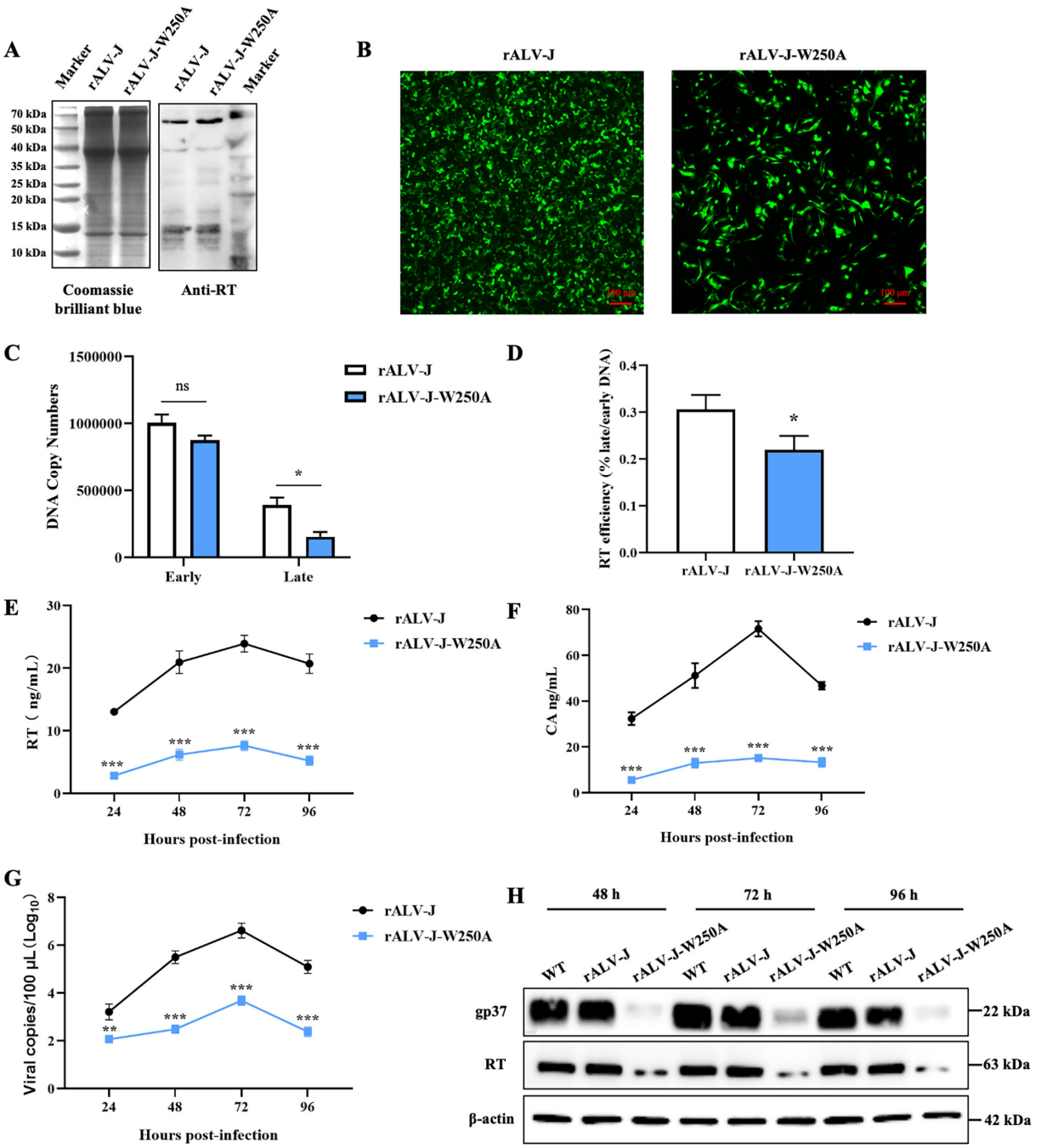

FIG 7 Residue W250 in the RT thumb domain is essential for ALV-J reverse transcription and replication. DF-1 cells were infected with rALV-J or rALV-J-W250A at an MOI of 0.01. Cells and culture supernatants were collected at the indicated time points for subsequent analyses. (A) Western blot analysis of purified virions. Recombinant viruses rALV-J and rALV-J-W250A were purified from cell supernatants via sequential clarification, filtration, ultracentrifugation, and sucrose cushion purification. Equal amounts of total viral protein were loaded for SDS-PAGE, followed by Western blotting with anti-RT antibody. Coomassie brilliant blue staining of the same gel served as a loading control. (B) Immunofluorescence analysis of viral protein expression. Cells were fixed at 72 hpi and stained with anti-gp37 antibody. Fluorescence signals were visualized using a fluorescence microscope. rALV-J was used as a reference. Scale bar, 100 µm. (C) qPCR analysis of viral DNA synthesis. Total cytoplasmic DNA was collected at 8 hpi. Early and late viral DNA copies were quantified by qPCR. (D) Reverse transcription efficiency. Reverse transcription efficiency was calculated as the ratio of late to early viral DNA copies, expressed as a percentage. (E) RT-assay signal. Cells were harvested at 24, 48, 72, and 96 hpi, and the RT-assay signal was quantified using a colorimetric reverse transcriptase assay. (F) ELISA analysis of viral CA secretion. Culture supernatants were collected at 24, 48, 72, and 96 hpi, and CA levels were measured by ELISA. (G) qPCR analysis of viral genome copies. Cells were harvested at 24, 48, 72, and 96 hpi, and intracellular viral genome copies were quantified by qPCR. (H) Western blot analysis of viral protein expression. Cell lysates were collected at 48, 72, and 96 hpi, and protein expression was detected using anti-gp37 and anti-RT antibodies. Endogenous β-actin served as a loading control. Western

(Continued on next page)

Fig 7 (Continued)

blots and immunofluorescence images are representative of at least three independent experiments with consistent results. Quantitative data are presented as mean ± SD from three independent biological replicates, each assayed in technical triplicate. Statistical significance was determined using unpaired two-tailed Student's *t*-tests. **P* < 0.05, ***P* < 0.01, and ****P* < 0.001.

the EKR residues of eEF1A are critical for supporting replication of all four ALV subgroups examined (ALV-A, ALV-B, ALV-K, and ALV-J), highlighting the broad-spectrum regulatory role of eEF1A across different ALV subgroups.

DISCUSSION

In our previous proteomic study, we consistently detected eEF1A in purified ALV-J virion preparations (19). We acknowledge that this observation does not by itself establish active or selective packaging of eEF1A. As a highly abundant cytosolic protein associated with cortical actin, eEF1A could potentially be incorporated passively during viral assembly and budding, analogous to the documented interaction between eEF1A and HIV-1 Gag (25). Regardless of the mechanism of virion association, the consistent detection of eEF1A prompted us to investigate its functional role during ALV-J replication. In this study, we demonstrate that eEF1A promotes ALV-J replication and associates with ALV-J RT to promote efficient reverse transcription. We further identify residues that are important for this association, including three key residues (E124, K129, and R134) within domain I of eEF1A and a hydrophobic pocket centered on W250 in the RT thumb domain. Disruption of this interface through mutagenesis severely compromises ALV-J reverse transcription and replication. To our knowledge, this study is the first to report that eEF1A acts as a key regulatory factor for ALV-J lifecycle, promoting viral proliferation by enhancing the reverse transcription efficiency.

Interestingly, a past study using protein fractionation combined with endogenous reverse transcription assay has identified that eEF1A is an important component of the HIV RTC. When the expression of eEF1A protein in cells is reduced using siRNA, the efficiency of HIV reverse transcription also significantly decreases (29). These findings provide the first evidence that orthologous host proteins facilitate reverse transcription across different retroviral genera, suggesting that recruitment of eEF1A may represent an evolutionarily conserved strategy to enhance replication efficiency. It is, therefore, plausible that an analogous eEF1A-dependent mechanism may operate in other retroviruses beyond HIV and ALV, an intriguing possibility that warrants future investigation. In addition, we found that eEF1A associates not only with ALV-J RT but also with viral integrase (IN) and protease (PR) (Fig. 2A). These interactions raise the possibility that eEF1A participates in multiple early stages of the retroviral life cycle. RT is the core component of the RTC, while IN is the catalytic core of the pre-integration complex (PIC). During the ALV-J replication process, the RTC is a dynamic structure that undergoes continuous remodeling during reverse transcription, with host proteins associating and dissociating at various stages (30–32). Upon completion of reverse transcription, the RTC undergoes structural rearrangement to form the PIC, accompanied by changes in its host protein composition. Finally, with the assistance of the PIC, the double-stranded DNA integrates into the host chromosomes, thereby completing the continuous and dynamic process from reverse transcription to integration (30). Our results suggest that eEF1A may remain associated throughout the transition from RTC to PIC without dissociating. A similar persistent association has been reported for human eEF1A with both HIV RT and IN, though molecular details remain limited (31). Moreover, eEF1A also plays an important role in the uncoating of the HIV viral core following entry (33, 34). Retroviral uncoating is a process during which incoming retroviral cores are altered to allow the integration of the viral genome into host chromosomes (35). Previous studies showed that the uncoating process of retroviruses relies on viral proteases (PR) to cut the Gag protein (36), and eEF1A also interacts with PR according to our results (Fig. 2A). Together, these findings suggest that eEF1A may function not only during

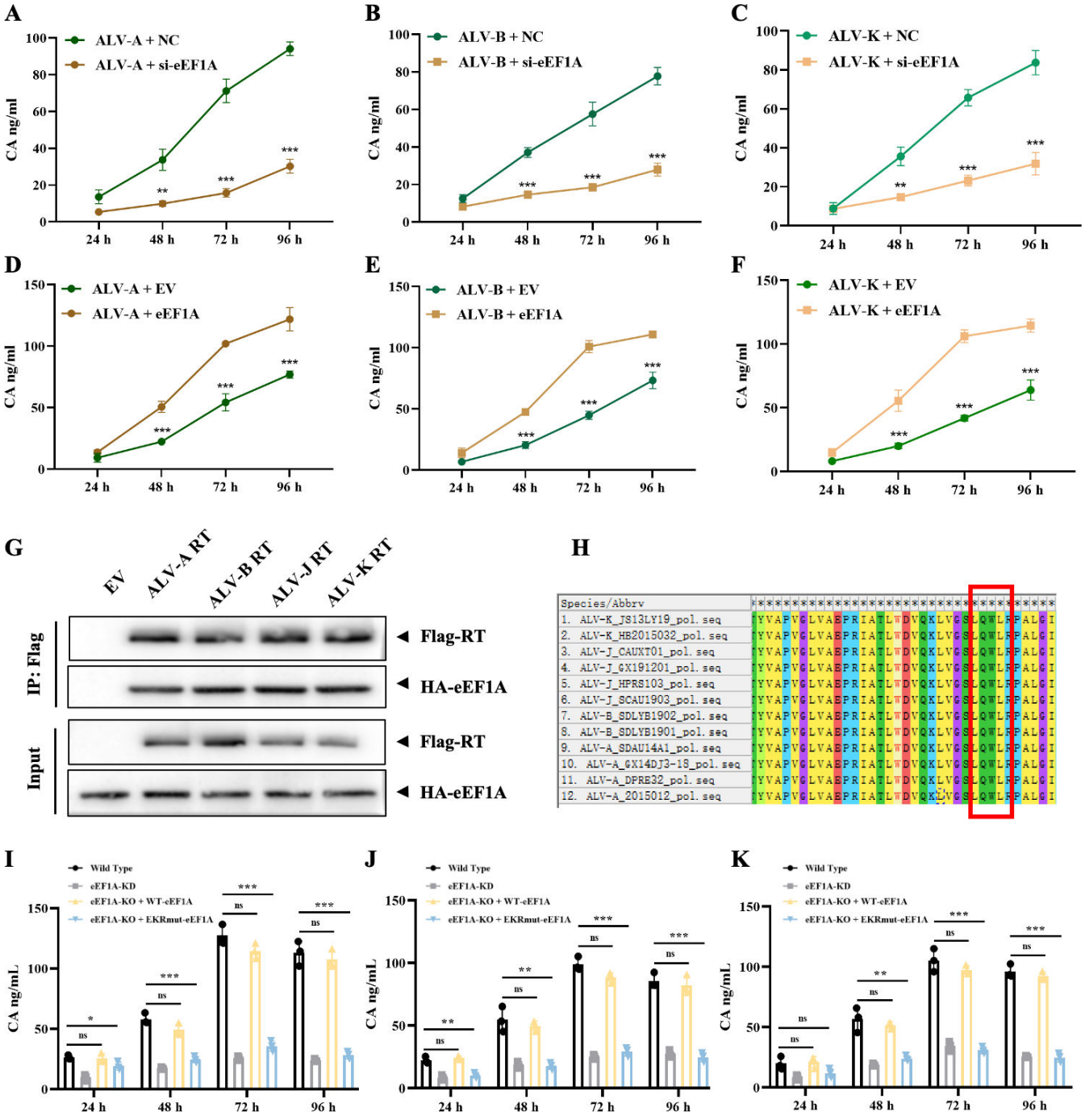

FIG 8 The eEF1A-RT interaction is conserved across multiple ALV subgroups. For knockdown experiments, DF-1 cells were transfected with si-NC or si-eEF1A. For overexpression experiments, DF-1 cells were transfected with EV or eEF1A overexpression plasmid. At 24 h post-transfection, cells were infected with ALV-A, ALV-B, ALV-J, or ALV-K at an MOI of 0.01. For rescue experiments, stable eEF1A-KD DF-1 cells were transfected with eEF1A-WT, eEF1A-EKRmut, or EV for 24 h, followed by virus infection. Normal DF-1 cells were included as a control. (A–C) ELISA analysis of viral CA secretion upon eEF1A depletion. DF-1 cells were transfected with si-eEF1A or si-NC and infected with ALV-A (A), ALV-B (B), or ALV-K (C). Culture supernatants were collected at the indicated time points, and CA levels were quantified by ELISA. (D–F) ELISA analysis of viral CA secretion upon eEF1A overexpression. DF-1 cells were transfected with the eEF1A overexpression plasmid or EV and infected with ALV-A (D), ALV-B (E), or ALV-K (F). Culture supernatants were collected at the indicated time points, and CA levels were quantified by ELISA. (G) Co-IP analysis of eEF1A interaction with RT proteins from different ALV subgroups. DF-1 cells were co-transfected with HA-tagged eEF1A and Flag-tagged RT constructs from ALV-A, ALV-B, ALV-J, or ALV-K. At 48 hpi, cell lysates were immunoprecipitated with anti-Flag antibody, followed by Western blotting with anti-HA and anti-Flag antibodies. (H) Sequence alignment of the RT thumb domain across ALV subgroups. Alignment of the thumb domain region

(Continued on next page)

Fig 8 (Continued)

of RT proteins from ALV-A, ALV-B, ALV-J, and ALV-K. The conserved tryptophan residue corresponding to W250 in ALV-J RT is highlighted. (I–K) Rescue of viral replication by wild-type eEF1A but not the EKR mutant in eEF1A-KD cells. Stable eEF1A-KD DF-1 cells were transfected with eEF1A-WT, eEF1A-EKRmut, or EV, followed by infection with ALV-A (I), ALV-B (J), or ALV-K (K). Culture supernatants were collected at the indicated time points, and CA levels were quantified by ELISA. Normal DF-1 cells were included as a control. Western blot images are representative of at least three independent experiments with consistent results. Quantitative data are presented as mean ± SD from three independent biological replicates, each assayed in technical triplicate. Statistical significance was determined using unpaired two-tailed Student's *t*-tests or one-way ANOVA, as appropriate. *P < 0.05, **P < 0.01, and ***P < 0.001, while "ns" indicates non-significance.

the core reverse transcription process but also throughout the entire viral replication cascade from uncoating to integration. Our ongoing efforts are aimed at delineating the dynamic role of eEF1A throughout the early stages of the replication cycle, which would significantly advance our understanding of core retroviral replication mechanisms.

We identified three key residues—E124, K129, and R134—within domain I of eEF1A that are essential for the RT association and thereby critical for viral reverse transcription and replication (Fig. 4 and Fig. 6). Domain I of eEF1A is the canonical GTP-binding and aminoacyl-tRNA binding domain, responsible for the factor's primary function in translation elongation by delivering the charged tRNA to the ribosome (20, 21). Domains II and III are primarily involved in mediating eEF1A's interactions with other cellular components, such as the ribosome (via domain II) and the actin cytoskeleton or signaling molecules (via the hypervariable C-terminal domain III) (20, 21, 37). The specific involvement of domain I in the RT association indicates that ALV-J targets a core, evolutionarily conserved region of eEF1A. Notably, the three residues we identified (E124, K129, and R134) lie outside both the canonical GTP-binding motif and the aminoacyl-tRNA-binding surface of domain I, suggesting that mutation of these residues would disrupt the association with RT without substantially compromising the essential translation-elongation function of eEF1A. The specific targeting likely reflects an adaptive viral strategy, which exploits an essential host function that is less prone to mutation without compromising cell viability. This may explain the broad-spectrum requirement for eEF1A across multiple ALV subgroups (ALV-A, -B, -K, and -J), all of which we found to be dependent on eEF1A for efficient replication activity (Fig. 8). Our attempt to generate a complete eEF1A knockout in DF-1 cells was unsuccessful due to the essential role of eEF1A in cell viability (Fig. 6A), consistent with prior studies demonstrating that complete eEF1A ablation is lethal across vertebrate systems (20, 29, 31). This underscores its nonredundant function in fundamental cellular processes; the residual wild-type alleles observed in the edited pool likely arise from a mix of incomplete editing, aneuploidy, and selective pressure against biallelic knockout cells. However, small RNA-mediated knockdown is a viable strategy that does not significantly impair cell viability, as demonstrated by our data and supported by previous studies (Fig. S1) (29, 31). We, therefore, propose that future efforts should prioritize precision gene-editing approaches to introduce subtle, interaction-disrupting mutations at the endogenous eEF1A locus in chickens, thereby disrupting their interaction with viruses without damaging their important physiological functions.

We also sought to identify the critical region within RT responsible for the eEF1A association. Deletion mapping revealed that the thumb domain of RT is important for the association as its removal substantially reduced the association, while deletion of both the thumb and connection domains abolished it entirely (Fig. 5B). The thumb domain, together with the fingers and palm domains, forms the canonical DNA polymerase active site cleft (30, 38). Beyond its structural role, the thumb domain is dynamic and intimately involved in positioning the template-primer, facilitating processivity, and coordinating the transition between polymerase and RNase H activities (30, 38). The connection domain acts as a flexible linker between the polymerase and RNase H domains, contributing to the overall conformational stability of the enzyme and influencing its interactions with nucleic acids and potential co-factors (30). Notably, research on HIV-1 has established that its RT thumb domain serves as a critical binding

platform for the human ortholog of eEF1A, with surface-exposed acidic residues of the thumb domain being essential for this interaction (29, 31, 35). We, therefore, postulated that the ALV-J RT thumb domain would harbor a functionally analogous, though likely not identical, binding site. Fine-scale mutagenesis within the thumb domain identified a single, conserved tryptophan residue (W250) that is critical for the interaction (Fig. 5). Introduction of a W250A mutation into an ALV-J infectious clone confirmed that this residue is important for both the eEF1A association and efficient viral reverse transcription and replication (Fig. 7). We acknowledge that alanine substitutions can, in principle, affect the co-immunoprecipitation signal indirectly, through altered folding, stability, solubility, or antibody accessibility; however, the concordant loss of association together with the functional defects in reverse transcription and replication observed with the W250A infectious clone support a specific contribution of W250 to the eEF1A association. These results reinforce the evolutionary conservation of eEF1A-mediated regulation of retroviral reverse transcription.

Our mutagenesis data convergently identify the E124/K129/R134 cluster in eEF1A domain I and W250 in the RT thumb domain as the functional core of the interaction interface. We note that molecular docking predictions do not unambiguously resolve a direct side-chain pairing between these residues, and our proposed structural model is, therefore, primarily supported by biochemical and functional evidence rather than *in silico* predictions alone (Fig. 5H). Although the precise structural nature of this engagement requires further validation, it is plausible that the bulky, hydrophobic side chain of W250 serves as a central anchor, potentially burying into a cleft on eEF1A. The surrounding charged residues (E124, K129, and R134) could then stabilize this interaction through long-range electrostatic forces and the formation of specific hydrogen bonds or salt bridges with adjacent polar or charged residues in the RT pocket (Table S2). Actually, the spatial organization of hydrophobic and charged residues is a well-documented determinant of both binding affinity and specificity (39). Furthermore, the central role of hydrophobic residues in driving protein interactions is universally recognized, with studies showing remarkable correspondence between hydrophobic protein patches and protein-binding interfaces (40). Thus, the observed combination of a W250-centered hydrophobic pocket in RT and the EKR charged cluster in eEF1A provides a compelling structural rationale for both the affinity and specificity characterizing their interaction, effectively explaining our biochemical and functional data. We note that the *in silico* docking does not unambiguously assign W250 as the direct counterpart of E124/K129/R134 (Table S2); the proposed EKR-W250 pairing is, therefore, inferred primarily from our complementary mutagenesis data rather than from the docking model alone. More broadly, the evidence presented here demonstrates a functional association between eEF1A and RT; a direct, quantitative binding assay using purified recombinant proteins will be required to formally establish a direct physical interaction.

Currently, the development of disease-resistant poultry lines is a crucial strategy for the long-term control of ALV. In recent years, both our team and others have made significant progress in developing disease-resistant breeds by targeting ALV-specific receptors (41–44). Cell receptors such as Tva (for ALV-A/K entry) and Tvb (for ALV-B/D/E entry) exhibit natural polymorphisms, providing valuable genetic material for ALV-resistant chicken development (41–43). For example, the natural mutation at the Tva W33 site conferred the natural resistance of guineafowl to ALV-K (45). The receptor chNHE1 has been identified as essential for ALV-J entry, with the W38 amino acid being critical for virus-host cell recognition (46). This site is highly conserved across chicken breeds, making it unsuitable for traditional selective breeding. Researchers have overcome this limitation by using CRISPR/Cas9 technology to precisely edit the W38 site, effectively disrupting the entry function of ALV-J and generating chickens resistant to ALV-J (44). While these receptor-targeting strategies represent groundbreaking advances, their scope remains inherently limited by the genetic diversity of viral entry mechanisms among ALV subgroups. Resistance conferred against one subgroup (e.g., ALV-J via chNHE1 editing) does not extend to others (e.g., ALV-A or ALV-B), necessitating the

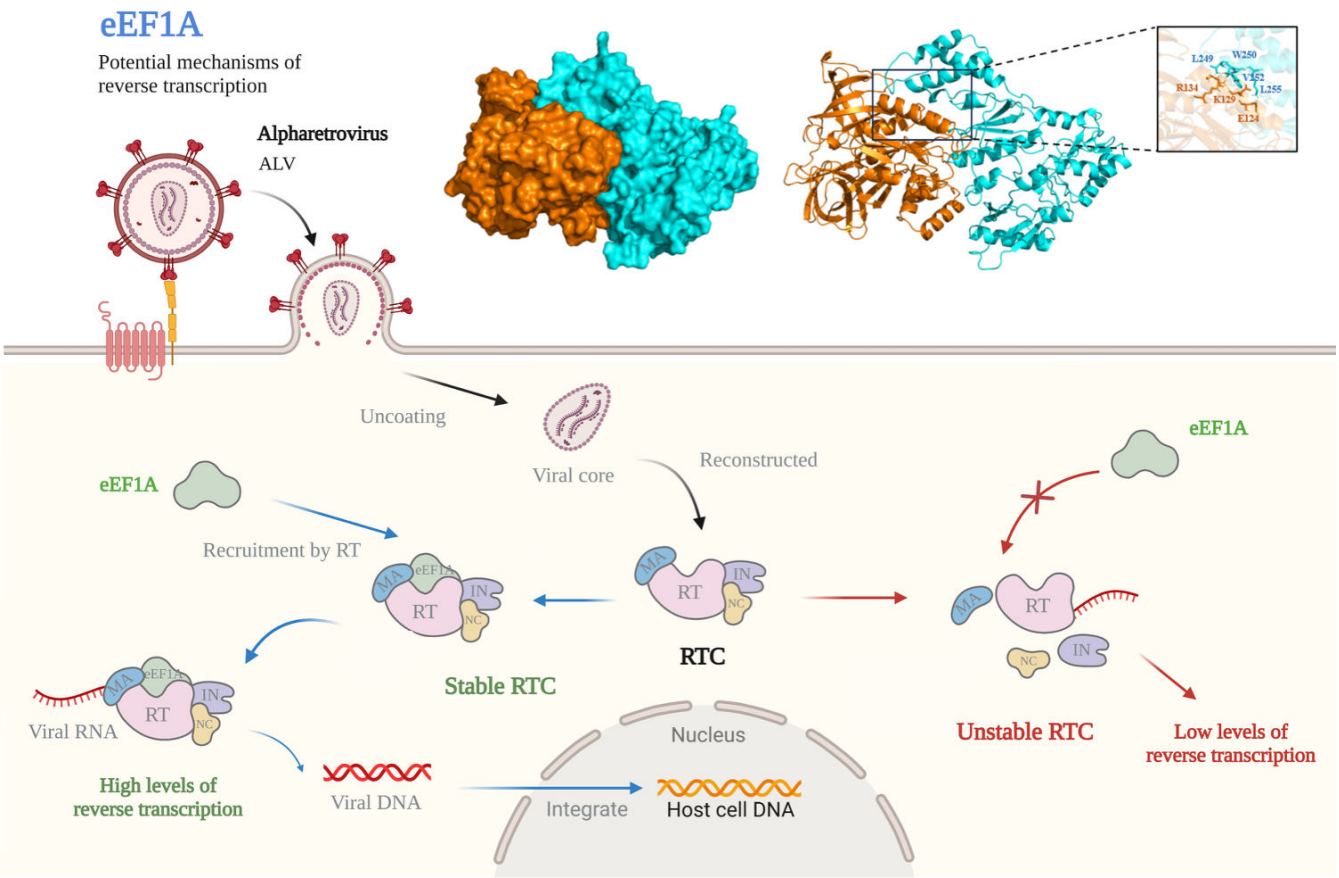

FIG 9 Schematic model of eEF1A-mediated regulation of ALV-J reverse transcription. This schematic illustrates the functional role of eEF1A in regulating ALV-J reverse transcription and replication. The molecular model (top) depicts the proposed association between the E124/K129/R134 cluster in eEF1A Domain I and the W250-centered hydrophobic pocket in the RT thumb domain. In normal cells (left), this association supports efficient reverse transcription and robust viral proliferation. In contrast, eEF1A-knockdown cells (right) exhibit impaired eEF1A-RT interaction, resulting in substantially reduced reverse transcription efficiency and viral replication.

development of multiple, subgroup-specific resistant lines. Moreover, the high variability of the envelope proteins enables the virus to undergo rapid adaptive changes, making it difficult for the resistance breeding efforts targeting receptor proteins to be sustained effective (47). In contrast to the variable entry receptors, the reverse transcription step is an indispensable and conservative stage in the life cycle of all ALV subgroups. Our study demonstrates that the viral RT, the core enzyme of this process, is highly conserved across ALV subgroups (Fig. 8). More importantly, we have identified the host factor eEF1A as a cofactor that associates with RT and promotes the viral replication efficiency of not only ALV-J but also ALV-A, ALV-B, and ALV-K (Fig. 3 and Fig. 8). Targeting this conserved eEF1A-RT interaction, therefore, represents a promising complementary strategy that could confer broad-spectrum resistance to multiple ALV subgroups simultaneously, complementing existing receptor-based approaches. Although any targeted residue can, in principle, mutate, W250 is buried within the hydrophobic core of the RT thumb domain and forms stabilizing contacts with neighboring residues (T248, D251, K254, and P285; Fig. 5I); mutation of this structurally constrained tryptophan is, therefore, expected to incur a substantial fitness cost that is unlikely to be readily compensated without impairing RT function. Unlike the variable, surface-exposed envelope proteins targeted by receptor-based strategies, the eEF1A-binding surface of RT represents a functionally indispensable, evolutionarily constrained interface that operates intracellularly; we, therefore, reason that this host-virus interface

may constitute a more escape-resistant antiviral target than receptor-based approaches, although this prediction awaits experimental validation.

Conclusions

In summary, our study identifies eEF1A as a critical host factor that associates with ALV-J RT via conserved residues E124, K129, and R134 in its domain I and W250 in the RT thumb domain, thereby enhancing reverse transcription efficiency and viral replication (Fig. 9). Notably, this interaction and its functional importance are conserved across multiple ALV subgroups (A, B, K, and J). These findings reveal a previously unrecognized host-virus interface essential for ALV replication and identify residues E124, K129, and R134 in eEF1A as potential targets for genome editing-based novel anti-ALV strategies.

ACKNOWLEDGMENTS

This research was funded by the Biological Breeding-National Science and Technology Major Project grant 2023ZD0405301, National Natural Science Foundation of China grants 32272981 and 32503009, Science and Technology Program of Guangdong Province grant 2023B0202010029, and Key Projects of Shaoguan University grant SZ2023KJ02.

Conceptualization: Sheng Chen and Qingmei Xie. Data curation: Sheng Chen, Liyi Chen, Huijuan Xu, and Liguo Gao. Formal analysis: Sheng Chen, Liyi Chen, Huijuan Xu, Yiming Yan, and Qingmei Xie. Funding acquisition: Sheng Chen, Yiming Yan, and Qingmei Xie. Investigation: Sheng Chen, Hongxin Li, Xinheng Zhang, Feng Chen, and Weiguo Chen. Methodology: Sheng Chen, Hongxin Li, Xinheng Zhang, Feng Chen, and Weiguo Chen. Project administration: Weiguo Chen and Qingmei Xie. Resources: Feng Chen. Supervision: Qingmei Xie. Writing – original draft: Sheng Chen, Weiguo Chen, and Qingmei Xie. Writing – review & editing: Sheng Chen, Weiguo Chen, and Qingmei Xie.

AUTHOR AFFILIATIONS

[1]State Key Laboratory of Swine and Poultry Breeding Industry & Guangdong Laboratory for Lingnan Modern Agriculture, College of Animal Science, South China Agricultural University, Guangzhou, China
[2]Guangdong Provincial Key Lab of Agro Animal Genomics and Molecular Breeding, Guangzhou, China
[3]Key Laboratory of Animal Health Aquaculture and Environmental Control, Guangdong, Guangzhou, China
[4]Henry Fok School of Biology and Agriculture, Shaoguan University, Shaoguan, China

AUTHOR ORCIDs

Sheng Chen http://orcid.org/0000-0001-8239-3132
Weiguo Chen http://orcid.org/0009-0005-5814-0190
Qingmei Xie http://orcid.org/0000-0001-6537-7798

FUNDING

Funder	Grant(s)	Author(s)
National Science and Technology Major Project	2023ZD0405301	Qingmei Xie
National Natural Science Foundation of China	32272981, 32503009	Qingmei Xie
Science and Technology Program of Guangdong	2023B0202010029	Qingmei Xie
Shaoguan University	SZ2023kj02	Yiming Yan

AUTHOR CONTRIBUTIONS

Sheng Chen, Conceptualization, Data curation, Formal analysis, Investigation, Methodology | Liyi Chen, Data curation, Formal analysis | Huijuan Xu, Data curation, Formal analysis | Liguo Gao, Data curation | Yiming Yan, Formal analysis | Hongxing Li, Investigation, Methodology | Xinheng Zhang, Investigation, Methodology | Feng Chen, Investigation, Methodology, Resources | Weiguo Chen, Investigation, Methodology, Project administration | Qingmei Xie, Conceptualization, Formal analysis, Project administration, Supervision

DATA AVAILABILITY

All data generated or analyzed during this study are included in this published article and its supplemental material (Mendeley Data, V2, doi: 10.17632/2rgtv8vsg4.2, https://data.mendeley.com/datasets/2rgtv8vsg4/2).

ADDITIONAL FILES

The following material is available online.

Supplemental Material

Fig. S1 to S2 and Tables S1 to S2 (JVI00925-26-S0001.docx). Fig. S1: siRNA reduced the expression level of eEF1A but did not affect cell viability. Fig. S2: The predicted binding mode of eEF1A and ALV-J RT. Table S1: The primers for constructing main plasmids and mutants. Table S2: Predicted binding sites of eEF1A to ALV-J RT.

REFERENCES

1. Chen W, Chen S, Nie Y, Li W, Li H, Zhang X, Chen F, Xie Q. 2022. Synergistic immunosuppression of Avian leukosis virus subgroup J and infectious bursal disease virus is responsible for enhanced pathogenicity. Viruses 14:2312. https://doi.org/10.3390/v14102312
2. Tan L, Li J, Duan Y, Liu J, Zheng S, Liang X, Fang C, Zuo M, Tian G, Yang Y. 2024. Current knowledge on the epidemiology and prevention of Avian leukosis virus in China. Poult Sci 103:104009. https://doi.org/10.1016/j.psj.2024.104009
3. Zhou D, Xue J, Zhang Y, Wang G, Feng Y, Hu L, Shang Y, Cheng Z. 2019. Outbreak of myelocytomatosis caused by mutational avian leukosis virus subgroup J in China, 2018. Transbound Emerg Dis 66:622–626. https://doi.org/10.1111/tbed.13096
4. Liu P, Li L, Jiang Z, Yu Y, Chen X, Xiang Y, Chen J, Li Y, Cao W. 2021. Molecular characteristics of subgroup J avian leukosis virus isolated from yellow breeder chickens in Guangdong, China, during 2016-2019. Infect Genet Evol 89:104721. https://doi.org/10.1016/j.meegid.2021.104721
5. Goto T, Nakai M, Ikuta K. 1998. The life-cycle of human immunodeficiency virus type 1. Micron 29:123–138. https://doi.org/10.1016/s0968-4328(98)00002-x
6. Campbell EM, Hope TJ. 2008. Live cell imaging of the HIV-1 life cycle. Trends Microbiol 16:580–587. https://doi.org/10.1016/j.tim.2008.09.006
7. Nisole S, Saïb A. 2004. Early steps of retrovirus replicative cycle. Retrovirology 1:9. https://doi.org/10.1186/1742-4690-1-9
8. Hu WS, Hughes SH. 2012. HIV-1 reverse transcription. Cold Spring Harb Perspect Med 2:a006882. https://doi.org/10.1101/cshperspect.a006882
9. Krupkin M, Jackson LN, Ha B, Puglisi EV. 2020. Advances in understanding the initiation of HIV-1 reverse transcription. Curr Opin Struct Biol 65:175–183. https://doi.org/10.1016/j.sbi.2020.07.005
10. Narayan S, Young JAT. 2004. Reconstitution of retroviral fusion and uncoating in a cell-free system. Proc Natl Acad Sci USA 101:7721–7726. https://doi.org/10.1073/pnas.0401312101
11. Lemay J, Maidou-Peindara P, Bader T, Ennifar E, Rain J-C, Benarous R, Liu LX. 2008. HuR interacts with human immunodeficiency virus type 1 reverse transcriptase, and modulates reverse transcription in infected cells. Retrovirology 5:47. https://doi.org/10.1186/1742-4690-5-47
12. Orlova M, Yueh A, Leung J, Goff SP. 2003. Reverse transcriptase of Moloney murine leukemia virus binds to eukaryotic release factor 1 to modulate suppression of translational termination. Cell 115:319–331. https://doi.org/10.1016/s0092-8674(03)00805-5
13. Wang X, Ao Z, Chen L, Kobinger G, Peng J, Yao X. 2012. The cellular antiviral protein APOBEC3G interacts with HIV-1 reverse transcriptase and inhibits its function during viral replication. J Virol 86:3777–3786. https://doi.org/10.1128/JVI.06594-11
14. Priet S, Navarro JM, Gros N, Querat G, Sire J. 2003. Functional role of HIV-1 virion-associated uracil DNA glycosylase 2 in the correction of G:U mispairs to G:C pairs. J Biol Chem 278:4566–4571. https://doi.org/10.1074/jbc.M209311200
15. Lemay J, Maidou-Peindara P, Cancio R, Ennifar E, Coadou G, Maga G, Rain J-C, Benarous R, Liu LX. 2008. AKAP149 binds to HIV-1 reverse transcriptase and is involved in the reverse transcription. J Mol Biol 383:783–796. https://doi.org/10.1016/j.jmb.2008.08.055
16. Kattenhorn LM, Mills R, Wagner M, Lomsadze A, Makeev V, Borodovsky M, Ploegh HL, Kessler BM. 2004. Identification of proteins associated with murine cytomegalovirus virions. J Virol 78:11187–11197. https://doi.org/10.1128/JVI.78.20.11187-11197.2004
17. Neuman BW, Joseph JS, Saikatendu KS, Serrano P, Chatterjee A, Johnson MA, Liao L, Klaus JP, Yates JR III, Wüthrich K, Stevens RC, Buchmeier MJ, Kuhn P. 2008. Proteomics analysis unravels the functional repertoire of coronavirus nonstructural protein 3. J Virol 82:5279–5294. https://doi.org/10.1128/JVI.02631-07
18. Lussignol M, Kopp M, Molloy K, Vizcay-Barrena G, Fleck RA, Dorner M, Bell KL, Chait BT, Rice CM, Catanese MT. 2016. Proteomics of HCV virions reveals an essential role for the nucleoporin Nup98 in virus morphogenesis. Proc Natl Acad Sci USA 113:2484–2489. https://doi.org/10.1073/pnas.1518934113
19. Chen S, Yan Y, Gao L, Gao S, Feng K, Li H, Zhang X, Chen W, Chen F, Xie Q. 2023. Proteomic profiling of purified avian leukosis virus subgroup J particles. Vet Microbiol 284:109821. https://doi.org/10.1016/j.vetmic.2023.109821
20. Sasikumar AN, Perez WB, Kinzy TG. 2012. The many roles of the eukaryotic elongation factor 1 complex. Wiley Interdiscip Rev RNA 3:543–555. https://doi.org/10.1002/wrna.1118
21. Abbas W, Kumar A, Herbein G. 2015. The eEF1A proteins: at the crossroads of oncogenesis, apoptosis, and viral infections. Front Oncol 5:75. https://doi.org/10.3389/fonc.2015.00075
22. Vera M, Pani B, Griffiths LA, Muchardt C, Abbott CM, Singer RH, Nudler E. 2014. The translation elongation factor eEF1A1 couples transcription to

translation during heat shock response. eLife 3:e03164. https://doi.org/10.7554/eLife.03164
23. Zhang X, Shi H, Chen J, Shi D, Li C, Feng L. 2014. EF1A interacting with nucleocapsid protein of transmissible gastroenteritis coronavirus and plays a role in virus replication. Vet Microbiol 172:443–448. https://doi.org/10.1016/j.vetmic.2014.05.034
24. Liu Y, Zhang Y, Wang M, Cheng A, Yang Q, Wu Y, Jia R, Liu M, Zhu D, Chen S, et al. 2020. Structures and functions of the 3′ untranslated regions of positive-sense single-stranded RNA viruses infecting humans and animals. Front Cell Infect Microbiol 10:453. https://doi.org/10.3389/fcimb.2020.00453
25. Cimarelli A, Luban J. 1999. Translation elongation factor 1-alpha interacts specifically with the human immunodeficiency virus type 1 gag polyprotein. J Virol 73:5388–5401. https://doi.org/10.1128/JVI.73.7.5388-5401.1999
26. Wu-Baer F, Lane WS, Gaynor RB. 1996. Identification of a group of cellular cofactors that stimulate the binding of RNA polymerase II and TRP-185 to human immunodeficiency virus 1 TAR RNA. J Biol Chem 271:4201–4208. https://doi.org/10.1074/jbc.271.8.4201
27. Abbas W, Khan KA, Tripathy MK, Dichamp I, Keita M, Rohr O, Herbein G. 2012. Inhibition of ER stress-mediated apoptosis in macrophages by nuclear-cytoplasmic relocalization of eEF1A by the HIV-1 Nef protein. Cell Death Dis 3:e292. https://doi.org/10.1038/cddis.2012.32
28. Li D, Wei T, Jin H, Rose A, Wang R, Lin M-H, Spann K, Harrich D. 2015. Binding of the eukaryotic translation elongation factor 1A with the 5′UTR of HIV-1 genomic RNA is important for reverse transcription. Virol J 12:118. https://doi.org/10.1186/s12985-015-0337-x
29. Warren K, Wei T, Li D, Qin F, Warrilow D, Lin M-H, Sivakumaran H, Apolloni A, Abbott CM, Jones A, Anderson JL, Harrich D. 2012. Eukaryotic elongation factor 1 complex subunits are critical HIV-1 reverse transcription cofactors. Proc Natl Acad Sci USA 109:9587–9592. https://doi.org/10.1073/pnas.1204673109
30. Coté ML, Roth MJ. 2008. Murine leukemia virus reverse transcriptase: structural comparison with HIV-1 reverse transcriptase. Virus Res 134:186–202. https://doi.org/10.1016/j.virusres.2008.01.001
31. Li D, Wei T, Rawle DJ, Qin F, Wang R, Soares DC, Jin H, Sivakumaran H, Lin M-H, Spann K, Abbott CM, Harrich D. 2015. Specific interaction between eEF1A and HIV RT is critical for HIV-1 reverse transcription and a potential anti-HIV target. PLoS Pathog 11:e1005289. https://doi.org/10.1371/journal.ppat.1005289
32. Lanchy JM, Isel C, Keith G, Le Grice SF, Ehresmann C, Ehresmann B, Marquet R. 2000. Dynamics of the HIV-1 reverse transcription complex during initiation of DNA synthesis. J Biol Chem 275:12306–12312. https://doi.org/10.1074/jbc.275.16.12306
33. Müller TG, Zila V, Müller B, Kräusslich HG. 2022. Nuclear capsid uncoating and reverse transcription of HIV-1. Annu Rev Virol 9:261–284. https://doi.org/10.1146/annurev-virology-020922-110929
34. Guerrero JF, Lesko SL, Evans EL, Sherer NM. 2024. Studying retroviral life cycles using visible viruses and live cell imaging. Annu Rev Virol 11:125–146. https://doi.org/10.1146/annurev-virology-100422-012608
35. Rawle DJ, Li D, Swedberg JE, Wang L, Soares DC, Harrich D. 2018. HIV-1 uncoating and reverse transcription require eEF1A binding to surface-exposed acidic residues of the reverse transcriptase thumb domain. mBio 9:e00316-18. https://doi.org/10.1128/mBio.00316-18
36. Lehmann-Che J, Giron M-L, Delelis O, Löchelt M, Bittoun P, Tobaly-Tapiero J, de Thé H, Saïb A. 2005. Protease-dependent uncoating of a complex retrovirus. J Virol 79:9244–9253. https://doi.org/10.1128/JVI.79.14.9244-9253.2005
37. Ramesh R, Sattlegger E. 2020. Domain II of the translation elongation factor eEF1A is required for Gcn2 kinase inhibition. FEBS Lett 594:2266–2281. https://doi.org/10.1002/1873-3468.13803
38. Sharaf NG, Brereton AE, Byeon I-JL, Karplus PA, Gronenborn AM. 2016. NMR structure of the HIV-1 reverse transcriptase thumb subdomain. J Biomol NMR 66:273–280. https://doi.org/10.1007/s10858-016-0077-2
39. Desantis F, Miotto M, Di Rienzo L, Milanetti E, Ruocco G. 2022. Spatial organization of hydrophobic and charged residues affects protein thermal stability and binding affinity. Sci Rep 12:12087. https://doi.org/10.1038/s41598-022-16338-5
40. Rego NB, Xi E, Patel AJ. 2021. Identifying hydrophobic protein patches to inform protein interaction interfaces. Proc Natl Acad Sci USA 118:e2018234118. https://doi.org/10.1073/pnas.2018234118
41. Li X, Chen W, Zhang H, Li A, Shu D, Li H, Dai Z, Yan Y, Zhang X, Lin W, Ma J, Xie Q. 2018. Naturally occurring frameshift mutations in the *tvb* receptor gene are responsible for decreased susceptibility of chicken to infection with avian leukosis virus subgroups B, D, and E. J Virol 92:e01770-17. https://doi.org/10.1128/JVI.01770-17
42. Liao CT, Chen SY, Chen WG, Liu Y, Sun BL, Li HX, Zhang HM, Qu H, Wang J, Shu DM, Xie QM. 2014. Single nucleotide polymorphism variants within tva and tvb receptor genes in Chinese chickens. Poult Sci 93:2482–2489. https://doi.org/10.3382/ps.2014-04077
43. Chen W, Liu Y, Li H, Chang S, Shu D, Zhang H, Chen F, Xie Q. 2015. Intronic deletions of tva receptor gene decrease the susceptibility to infection by avian sarcoma and leukosis virus subgroup A. Sci Rep 5:9900. https://doi.org/10.1038/srep09900
44. Koslová A, Trefil P, Mucksová J, Reinišová M, Plachý J, Kalina J, Kučerová D, Geryk J, Krchlíková V, Lejčková B, Hejnar J. 2020. Precise CRISPR/Cas9 editing of the NHE1 gene renders chickens resistant to the J subgroup of avian leukosis virus. Proc Natl Acad Sci USA 117:2108–2112. https://doi.org/10.1073/pnas.1913827117
45. Gáliková E, Přikryl D, Prost S, Kučerová D, Trejbalová K, Hejnar J. 2025. Single amino acid residue W33 of *tva* receptor is critical for viral entry and high-affinity binding of avian leukosis virus subgroup K. Viruses 17:709. https://doi.org/10.3390/v17050709
46. Chai N, Bates P. 2006. Na+/H+ exchanger type 1 is a receptor for pathogenic subgroup J avian leukosis virus. Proc Natl Acad Sci USA 103:5531–5536. https://doi.org/10.1073/pnas.0509785103
47. Matoušková M, Plachý J, Kučerová D, Pecnová Ľ, Reinišová M, Geryk J, Karafiát V, Hron T, Hejnar J. 2024. Rapid adaptive evolution of avian leukosis virus subgroup J in response to biotechnologically induced host resistance. PLoS Pathog 20:e1012468. https://doi.org/10.1371/journal.ppat.1012468